Geochemistry, Geophysics, Geosystems

Supporting Information for

Fluvio-sedimentary response to late Quaternary climate and tectonics at the Main Frontal Thrust, central Nepal

Mari Hamahashi[1†], Judith A. Hubbard[1, 2], Rafael Almeida[3], Samuel H. Haines[1],

Lewis A. Owen[4], Sanjita Mishra[5], and Soma Nath Sapkota[5]

[1]Earth Observatory of Singapore, Nanyang Technological University, Singapore

[2]Asian School of the Environment, Nanyang Technological University, Singapore

[3]Department of Geological Sciences, San Diego State University, USA

[4]Department of Marine, Earth, and Atmospheric Sciences, North Carolina State University, USA

[5]Department of Mines and Geology, National Seismological Center, Nepal

[†]Now at Kobe University, Kobe Ocean-Bottom Exploration Center, Japan

Contents of this file

Text S1 to S2

Figures S1 to S8

Additional Supporting Information (Files uploaded separately)

Captions for Datasets S1 to S2

Introduction

This supporting information contains detailed descriptions of the dating methodologies employed in this study, and additional descriptions of the outcrop terraces and bedrock surrounding our study area. Text S1 contains the description of optically stimulated luminescence (OSL) dating methodology. Text S2 contains the description of radiocarbon (^{14}C) dating methodology. Figure S1 shows the uninterpreted image of the Ratu river seismic profile (pre-stack depth-migrated, no vertical exaggeration) by Almeida et al. (2018) with co-located boreholes P6-P10 in this study. Figures S2 and S3 illustrate the features of bedrock Upper Siwalik Group and outcrop terraces surrounding our study area. Figure S4 shows regional satellite map of the Himalayan foreland and Ganges plain illustrating the rivers studied in this paper and the surrounding major rivers. Figures S5 and S6 show data of measured luminescence and equivalent dose of samples and the analysis of two-mixing model used to obtain OSL age. Figure S7 shows the calibration data of radiocarbon age to calendar years. Figure S8 shows the locations of previous studies in other foreland regions cited in this paper. Dataset S1 contains our core description data (raw data) presented in this paper. Dataset S2 contains the geotechnical report created by the drilling company.

Text S1. Optically stimulated luminescence (OSL) dating

Eighteen OSL samples were chosen from relatively well-sorted, silt to fine sand identified from surrounding cores at Sites P2, P3, P4, P6, P7, and P9, and were measured for quartz OSL at the University of Cincinnati and North Carolina State University in the USA. We avoided poorly-sorted fluvial sediment (sand with pebbles) due to risk of partial bleaching during fluvial transport, and selected well-sorted fluvial sediment (silty sand to clay). The samples were opened in the Luminescence Dating Laboratory under safe light conditions. The end of each sample (approximately 1 inch) was first removed, and were dried to determine water content. The sediment from the ends were then crushed and sent to the Activation Laboratories Limited in Ancaster, Ontario, Canada for Major Elements Fusion ICP/MS/Trace Elements analysis to determine the U, Th, Rb and K concentrations for dose rate calculations (Table 2).

The remaining samples were pretreated with 10% HCl and 10% H_2O_2 to remove carbonates and organic matter, respectively. The pretreated samples were rinsed in water, dried and sieved to obtain the 90-150 μm particle size fraction. A sub-fraction (~20 g) of

each sample was etched using 44% HF acid for 80 minutes to remove the outer alpha irradiated layer from quartz particles. This treatment also helps dissolve any feldspars present. Any fluorides precipitated during HF treatment were removed using concentrated HCl for 30 min. The quartz samples were then rinsed in distilled water and acetate, and dried and sieved to obtain grain size 90-150 μm in diameter. Next, a low-field-controlled Frantz isodynamic magnetic separator (LFC Model-2) was used to separate feldspar and magnetic minerals from quartz in the 90-150 μm particle size fraction following the method of Porat (2006), with the forward and side slopes set at 100° and 10°, respectively, within a variable magnetic field. The quartz was sieved using a 90 μm mesh to remove any grains smaller than 90 μm, so that the 90-150 μm fraction could be used for OSL measurement.

An automated Riso OSL reader model TL-DA-20 was used for OSL measurements and irradiation. Aliquots, containing approximately several hundred grains of the samples, were mounted onto ~6 mm-diameter stainless steel discs as a small central circle of ~3 mm in diameter. Aliquots were first checked for feldspar contamination using infrared stimulated luminescence (IRSL) at room temperature before the main OSL measurements were undertaken (Jain and Singhvi, 2001). The samples that did not pass the IRSL test were etched in 40% HF for further 30 minutes to remove any feldspar, followed by 10% HCl treatment and sieving again. The samples then passed the IRSL test and was used for OSL dating. Aliquots of the samples were illuminated with blue LEDs stimulating at a wavelength of 470 nm (blue light stimulated luminescence). The detection optics comprised Hoya U-340 and Schott BG-39 color glass filters coupled to an EMI 9235 QA photomultiplier tube. The aliquots were irradiated using a $^{90}Sr/^{90}Y$ beta source. The single aliquot regeneration (SAR) method (Murray and Wintle, 2000; 2003) was used to determine the dose rate for age estimation. Only aliquots that satisfy the criterion of a recycling ratio not more than 10% were used in determining equivalent dose. A preheat of 240°C for 10 s was used and the OSL signal was recorded for 40 s at 125°C. OSL sensitivity of the samples had a high signal to noise ratio. Dose recovery tests (Wintle and Murray, 2006) indicate that a laboratory dose of 10 Gy could be recovered to within 10% by the SAR protocol, suggesting that the protocol was appropriate.

Table 2 presents the radioisotope, water content, and cosmic dose, dose rate, equivalent dose, and OSL age for the samples. Dose rate calculations follows the details highlighted in the captions of Table 2 and confirmed using the Dose Rate and Age Calculator (DRAC) of Duncan et al. (2015). The dose rates for the samples were 3.21±0.19 and 3.98±0.24 Gy/ka, which is within the normal range for terrestrial sediments. The Th/U

ratio is consistent with there being no problems of leaching of radionuclides from the sediment. Natural water content was ~10%, and we assumed a conservative value with a large uncertainty (±5%) to account for any possible changes in water content over the geologic history.

The natural OSL signal for all aliquots were at least two orders of magnitude greater than background signal. The shine down curves (luminescence stimulated in the lab over 40 s of exposure to light) for all aliquots showed fast decay patterns that confirm that the signal is the fast component of luminescence, which is dominant in quartz. This provides confidence that quartz would have likely been bleached quickly if only briefly exposed to sunlight. Figure S3 shows an example of shine down curves for the dated samples. Figure S3 also shows examples of the regenerative curves, illustrating good growth and recuperation. Dose rate recovery tests for the samples showed that they have good recovery within the uncertainty of the laboratory measurement and 10% of the applied dose of 100 s.

At least thirty-two aliquots were measured for each sample. Of those several aliquots were saturated (»200 Gy), and many aliquots failed the recuperation (especially for sample P3-39) and recycling criteria (Table 2). The remaining aliquots were used to determining a likely equivalent dose for the sample (Table 2). The spread of equivalent dose varied between the samples and are shown in Figure S4. In all the samples (especially P3-39), the large spread of equivalent dose values (dispersion >25%) and the significant number of aliquots that were saturated suggests partial bleaching problems (i.e., not all the sand grains were totally rest by sunlight before burial). This can result in an overestimate of the age. To address this issue, we use a minimum age model separating the population of equivalent dose using a two-mixing model (Figure S4; Vermeesch, 2009), and we use the equivalent dose value of the minimum peak to calculate the age (Table 2 and Figure S4). This provides best estimation of ages (see ages highlighted in bold in Table 2). For completeness and comparison, the average and weighted averages ages are provided in Table 2. The average ages are overestimates because of partial bleaching issue and have large uncertainties associated with them, but all our data is included in those ages. The weighted averages skew the ages towards the lower range because of the smaller associated uncertainties with low value aliquots. These ages are similar to the two-mixing model ages, adding confidence in our two-mixing model ages (Table 2). In this study, we use average OSL ages for samples that showed ≤ 25% dispersion of the aliquots, and 2-mixing model OSL ages for samples that yielded > 25% dispersion (Table 2).

Text S2. Radiocarbon (^{14}C) dating

Fourteen samples of organic sediment were retrieved from the cores at Sites P2, P3, and P8, and measured for ^{14}C dating at Beta Analytics Inc., following standard laboratory procedures. Given the absence of charcoals and other macrofossils, the bulk organic fraction (carbon content: 0.06-1.62%) of less than 180 µm in size, inclusive of humic and humins, were used for dating. The samples were first visually inspected for size, homogeneity, debris, inclusions, clasts, grain size, organic constituents and potential contaminants, before they were dispersed in de-ionized water and sieved through a 180 µm mesh. The samples were then bathed in 1.25 N HCl at 90°C for a minimum of 1.5 hours to ensure removal of carbonates, followed by serial de-ionized water rinses at 70°C until neutrality was reached. Any debris or micro-rootlets were discarded during these rinses. After drying in an oven at 100°C for 12-24 hours, HCl was applied to a representative sub-sample under the microscope to validate the absence of carbonate. Microscopic examination was performed to assess its characteristics and to determine the appropriate sub-sample for AMS dating.

The pretreated samples were then oxidized to CO_2 by combustion at 1000-1200°C. The CO_2 generated was cryogenically purified by removing water vapor and any non-combustible/condensable gases, and were converted to graphite (Vogel et al., 1984; Manning and Reid, 1977). AMS counting was performed by charging the atoms in the sample graphite using NEC accelerator mass spectrometers. Stable isotope ratio ($^{13}C/^{12}C$ or $\delta^{13}C$) values were measured separately by Thermo isotope ratio mass spectrometers (IRMS). The conventional radiocarbon age was calculated using the Libby half-life (5568 years), and were corrected for total isotopic fractionation effects. Errors reported from the laboratory are based on 1 sigma counting statistics, and the conventional ages and their sigmas were rounded to the nearest 10 years. Calibration of the conventional age were performed using the 2013 calibration databases (INTCAL13) (Reimer et al., 2013), high probability density range method and Bayesian probability analysis (Ramsey, 2009) (Fig. S5).

$\delta^{13}C$ values of bulk organic fraction can be referred as a proxy to infer intensity of regional precipitation, in the recognition that differences in $\delta^{13}C$ values of plants are controlled by differences in metabolic processes in C_3 and C_4 plants (e.g. Kohn, 2010). It serves as a proxy because C_3 plants are generally known to flourish under moderate temperature and wet climate, compared to C_4 plants which favor cold and dry climate (e.g. O'Leary, 1981; Farquhar et al. 1982). $\delta^{13}C$ values of C_3 plants are reported to range between -35 and -22‰, whereas C_4 plants range between -20 and -9‰ (e.g. Osmond et

al., 1982). In this study, we placed a cut-off around -15 to 20‰ to infer differences in C_3 and C_4 plants and climate.

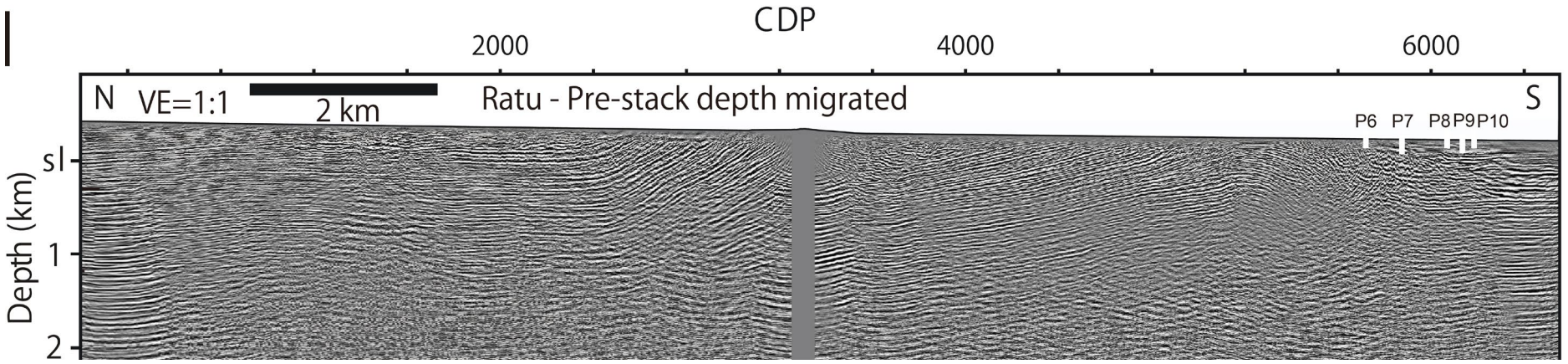
CDP
2000
4000
6000
N
VE=1:1
2 km
Ratu - Pre-stack depth migrated
S
P6
P7
P8
P9
P10
Depth (km)
sl
1
2

Figure S1. Ratu river seismic profile (pre-stack depth-migrated, no vertical exaggeration) by Almeida et al. (2018), uninterpreted image. CDP spacing is 2.5 m. Depth measurements are with respect to sea level (sl). White vertical bars show location of borehole sites P6–P10 in this study. Interpretation by Almeida et al. (2018) is shown in Figure 3a (main text).

a

Bedrock (Upper Siwalik Group)

Consist of sandstone, siltstone, gravels, interlayers of silt and sand

b

Strath terrace

(Incision of bedrock)

Fill terrace

(Deposition-dominant)

c

Sedimentary processes in fluvial sediments

(arrows: bedding orientation)

Incision of gravels into finer sediments

Deposition and cross-bedding

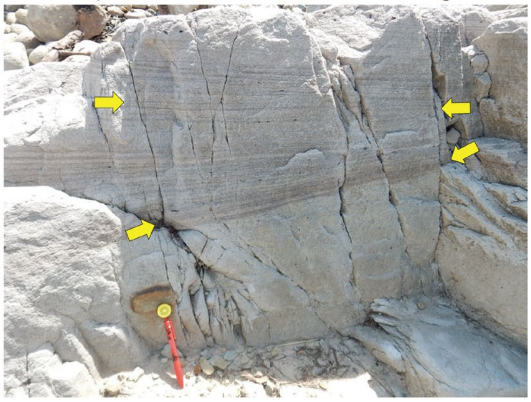

Figure S2. (a) Representative images of bedrock Upper Siwalik Group observed from the outcrops in the study area. Left panel: Gray silt (partially oxidized). Right panel: Grayish orange silt and fine sand. **(b)** Representative images of terrace outcrops in the study area. Left panel: Features of a strath terrace, showing tilted Upper Siwalik bedrock (sandstones) incised and buried by more recent fluvial sediments (gravels), bounded by white dotted line. Right panel: Features of a fill terrace, showing thick sequence of recent fluvial sediments, interbedded with fine sand/gravels (bounded by white dotted lines). The bedrock is not exposed in fill terraces. **(c)** Representative images of terrace outcrops showing sedimentary processes in fluvial sediments. Yellow arrows mark bedding orientations. Left panel: Beveled erosional surface between finer and coarser fluvial sediments. Right panel: Cross-bedding observed in sandstone.

Observation from outcrop terraces

Outcrop photo location

(a) Elevation across i-i'

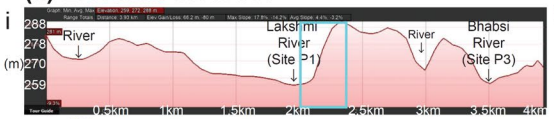

Terrace consist of alluvial fill sediments

(b) Elevation across ii-ii'

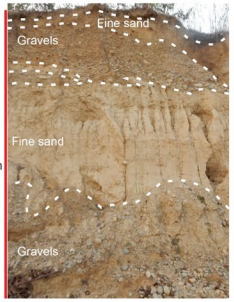

Terrace adjacent to river:
Interlayers of fine sand and gravels

(c) Elevation across iii-iii'

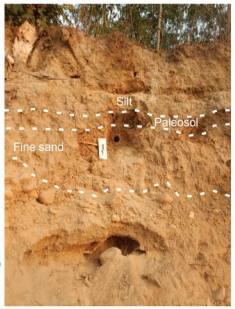

Well-sorted silt (aeolian?), paleosol,
fine sand and gravels (fluvial)

(d) Elevation across iv-iv'

Well-sorted silt (aeolian?), fine sand and gravels (fluvial)

(e) Elevation across v-v'

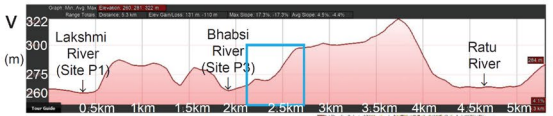

Older terrace sediments are red in color

Figure S3. Views of exposures along river terraces surrounding borehole sites in this study. Map shows locations of borehole Sites P1-P3. Blue lines in map show locations of elevation profiles for (a)-(e). **(a)** Elevation profile across i-i′ and representative images of river terrace outcrops along the Lakshmi River (location is indicated in blue box in elevation profile). River terrace sediments consist of mainly alluvial fill sediments. **(b)** Elevation profile across i-ii′ and representative images of terrace outcrops along the Bhabsi River (location is indicated in blue box in elevation profile). River terrace sediments consist of interlayers of fine sand and gravels. **(c)** Elevation profile across iii-iii′ and representative images of terrace outcrops along the Lakshmi River (location is indicated in blue box in elevation profile). River terrace sediments consist of well-sorted silt, paleosol, fine sand and gravels. **(d)** Elevation profile across iv-iv′ and representative images of terrace outcrops along the Lakshmi River (location is indicated in blue box in elevation profile). Terrace sediments consist of well-sorted silt, fine sand and gravels. **(e)** Elevation profile across v-v′ and representative images of terrace outcrops along the Bhabsi River (location is indicated in blue box in elevation profile). Terrace consist of alluvial fill sediments.

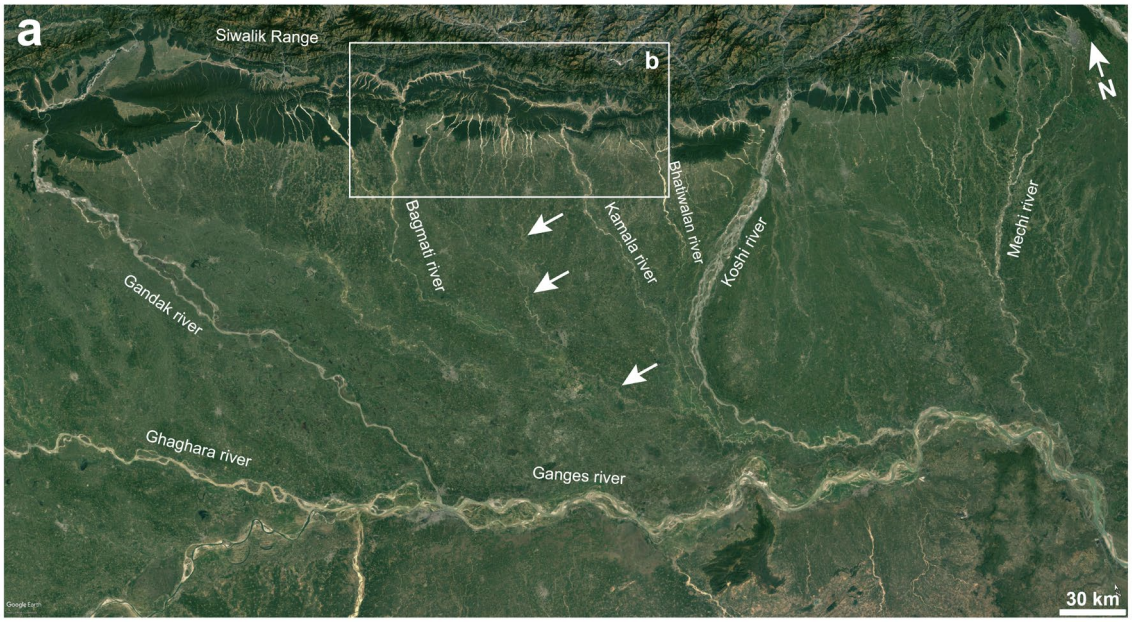

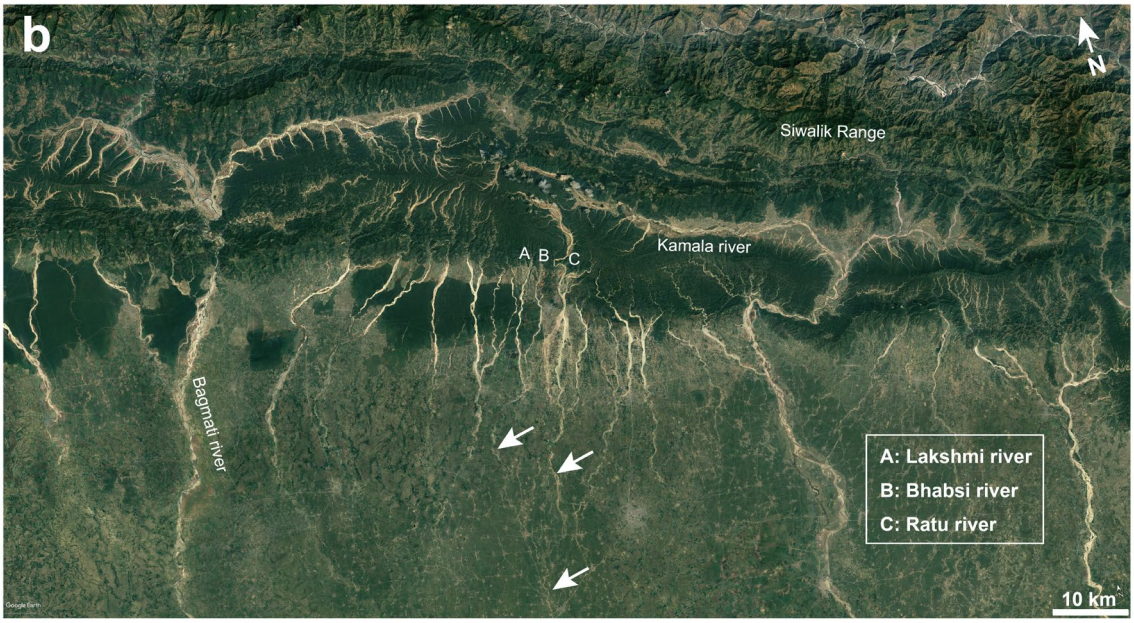

Figure S4. Regional satellite image showing the rivers studied in this paper and the surrounding major rivers flowing into the Himalayan foreland and to the Ganges plain. **(a)** In contrast to the major transverse Himalayan rivers such as the Koshi, Gandak, and the Ganges rivers, which have large drainage basins further upstream (High Himalaya), the drainage of the rivers in this study (white square closed-up in b.) are limited to the southern part of the Siwalik Range and are smaller ("footwall-fed rivers"). As the rivers travel hundreds of kilometers towards the southeast, their channel widths decrease (white arrows). Some of the channels are abandoned, while some merge with the Koshi and the Ganges rivers. **(b)** Close-up map showing the rivers in this study and their drainage basins within the Siwalik Range. A: Lakshmi river. B: Bhabsi river. C: Ratu river. The width of the rivers decreases downstream (white arrows). Satellite image uses map from Google Earth imagery, Image Landsat/Copernicus.

P3-31M

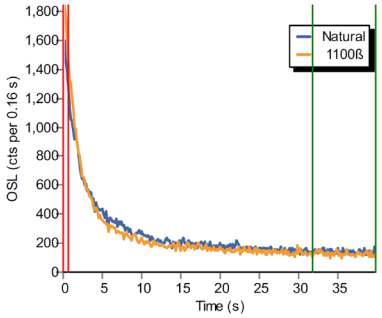

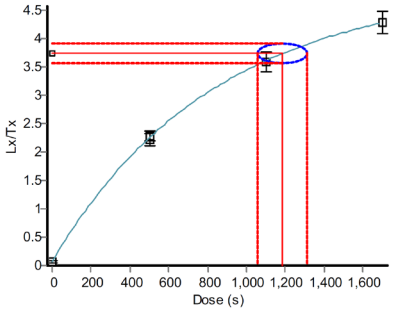

P3-39M

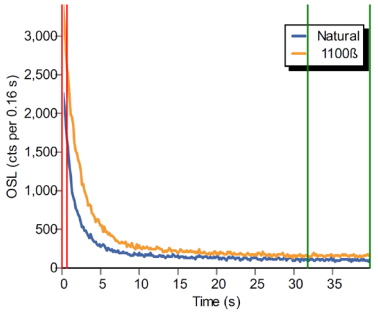

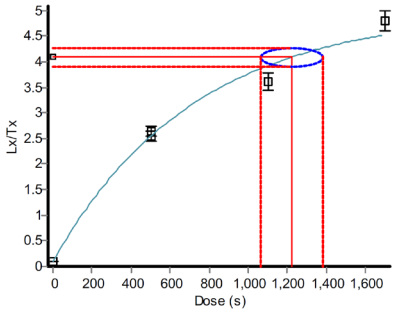

P3-41M

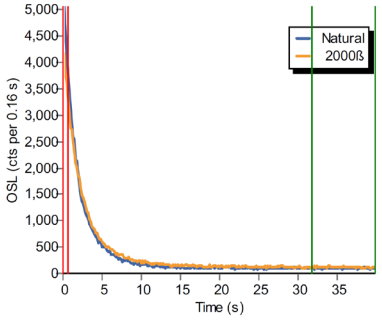

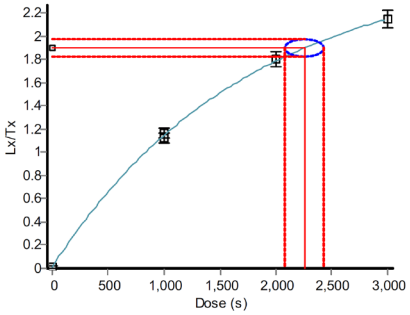

P3-49M

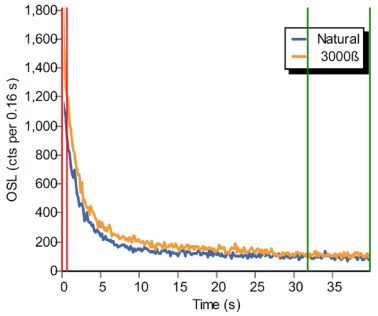

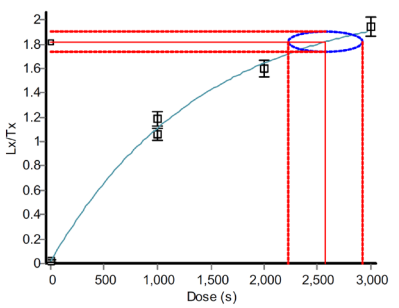

P2-23m

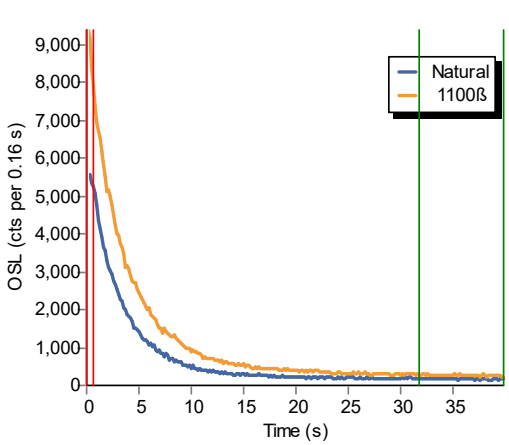
Natural
1100ß
OSL (cts per 0.16 s)
Time (s)

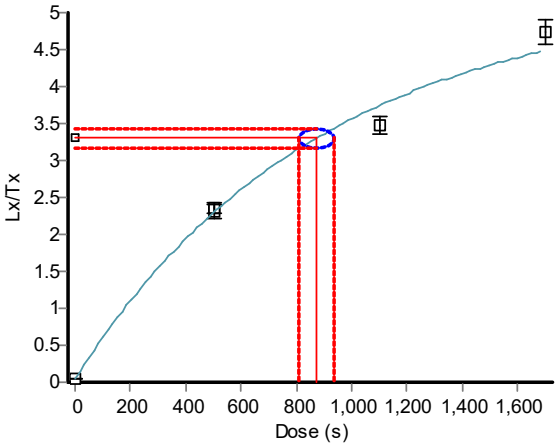
Lx/Tx
Dose (s)

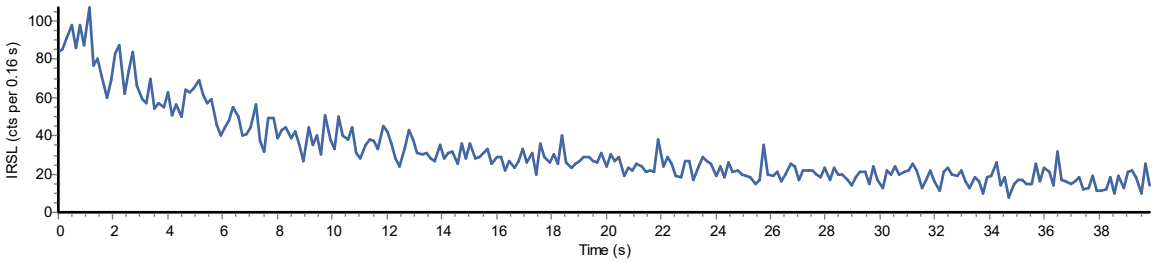
IRSL (cts per 0.16 s)
Time (s)

P2-27m

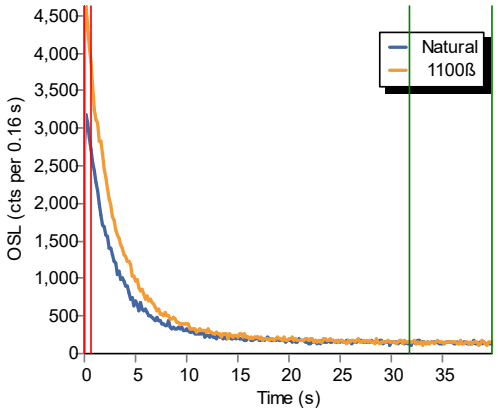
Natural
1100ß
OSL (cts per 0.16 s)
Time (s)

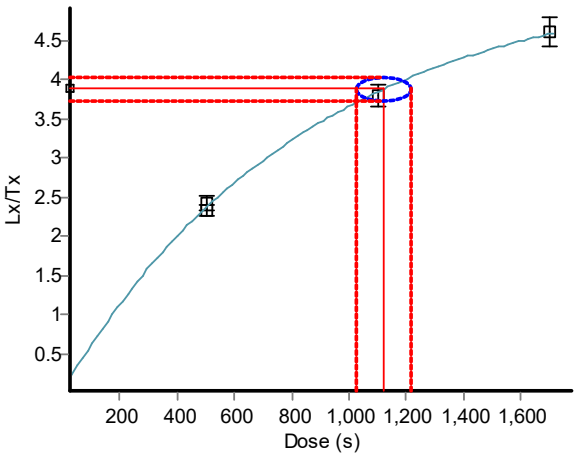
Lx/Tx
Dose (s)

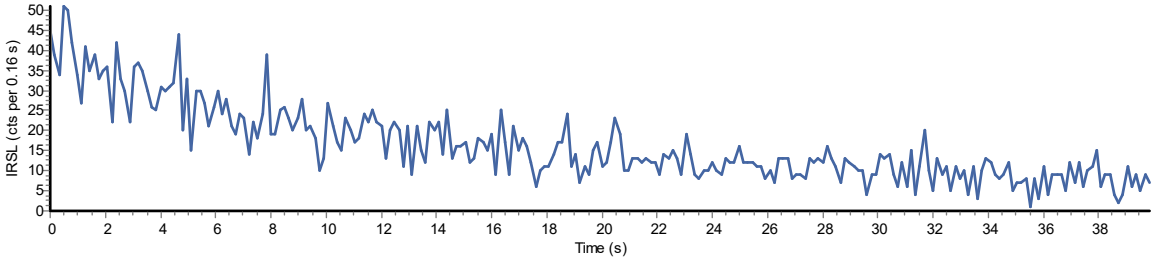
IRSL (cts per 0.16 s)
Time (s)

P2-31m

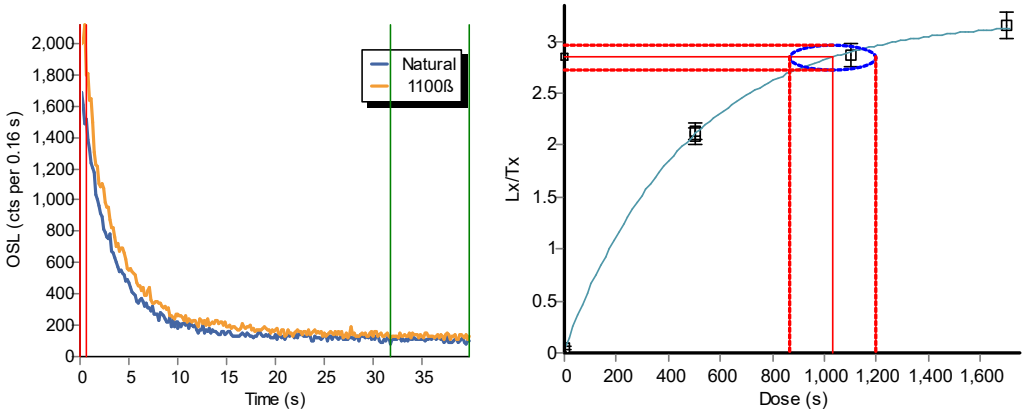
Natural
1100ß
OSL (cts per 0.16 s)
Time (s)
Lx/Tx
Dose (s)

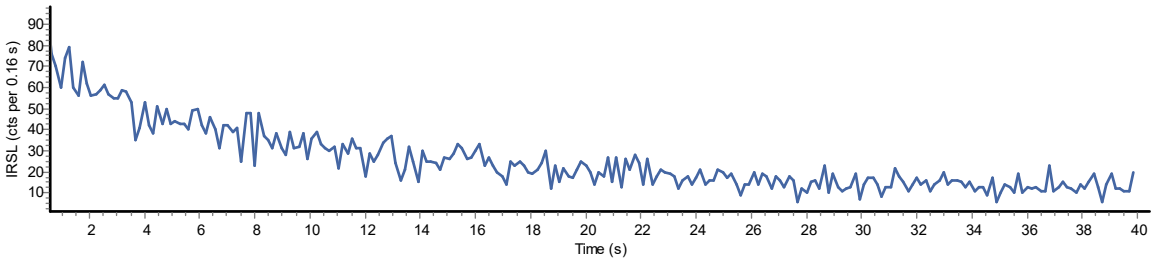
IRSL (cts per 0.16 s)
Time (s)

P2-31 (Representative saturated curve)

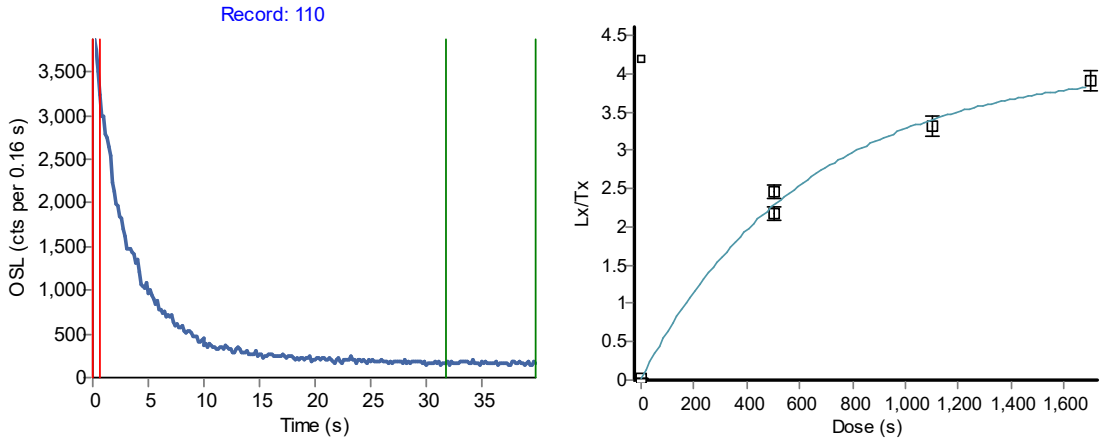

P2-41m

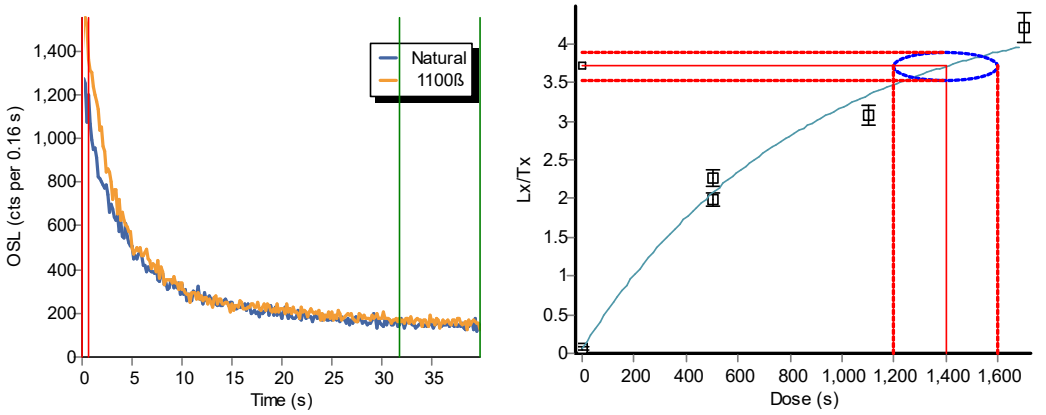

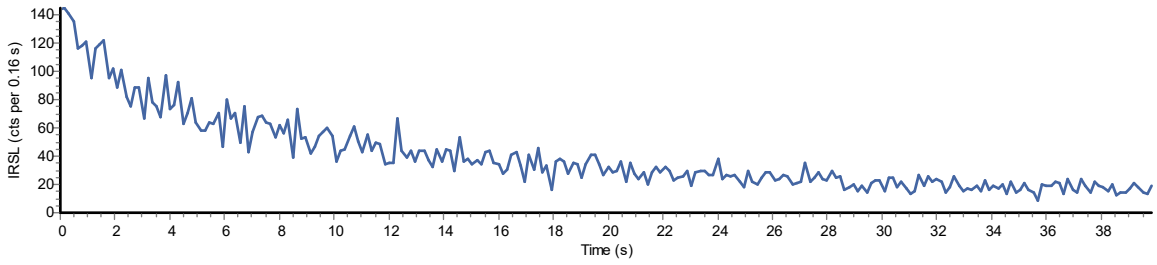

P2-41 (Representative saturated curve)

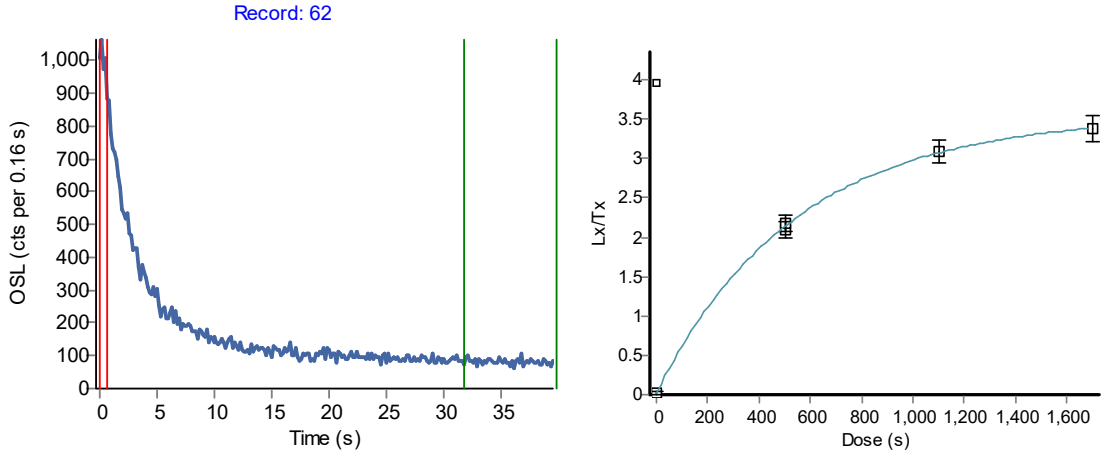

P3-29m

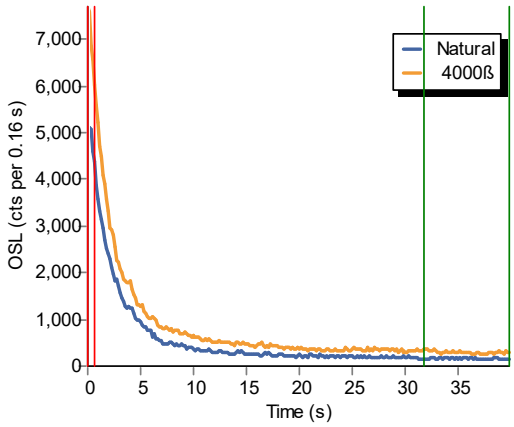
Natural
4000ß
OSL (cts per 0.16 s)
Time (s)

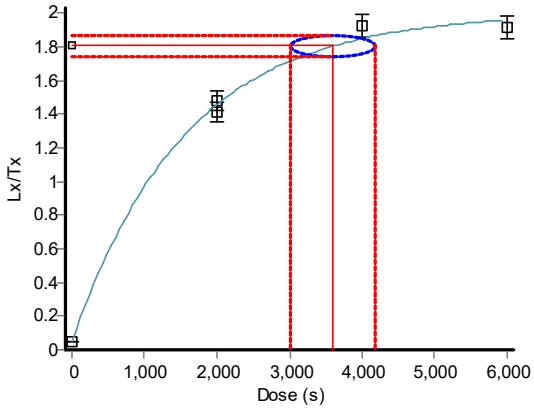
Lx/Tx
Dose (s)

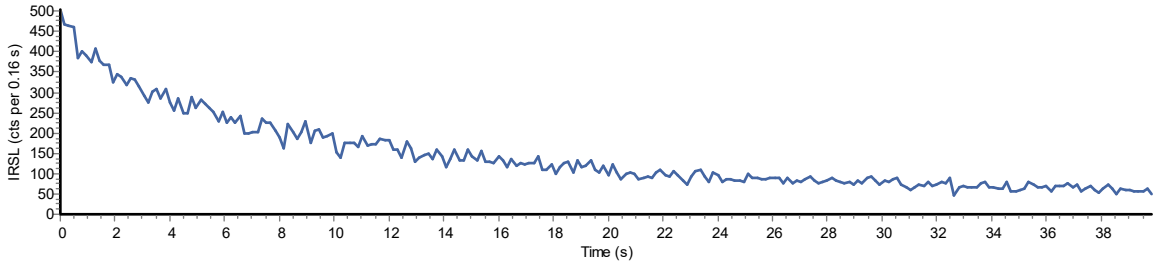
IRSL (cts per 0.16 s)
Time (s)

P4-51m

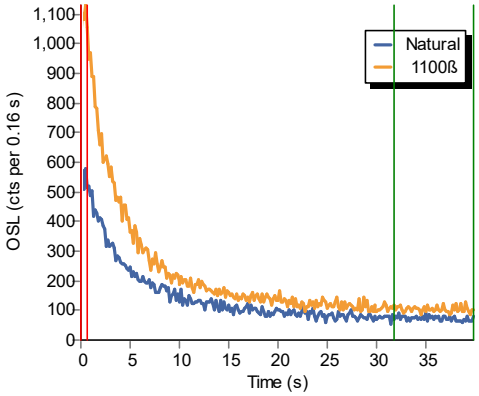
Natural
1100ß
OSL (cts per 0.16 s)
Time (s)

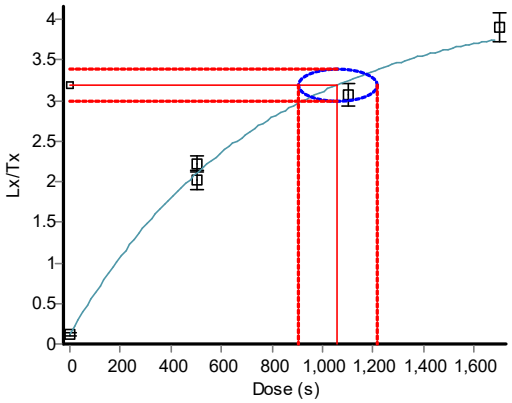
Lx/Tx
Dose (s)

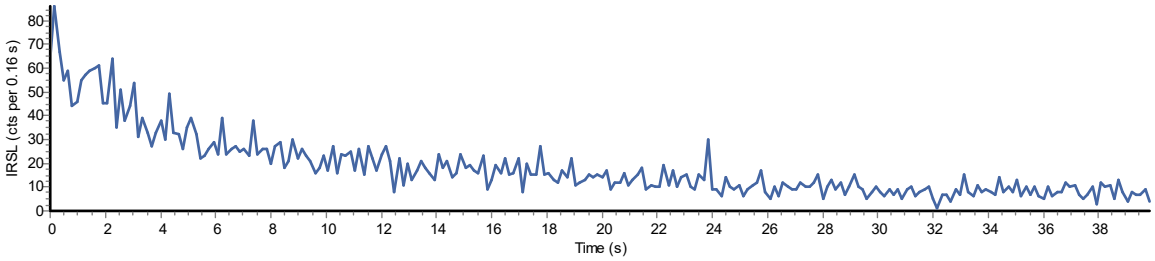
IRSL (cts per 0.16 s)
Time (s)

P4-69m

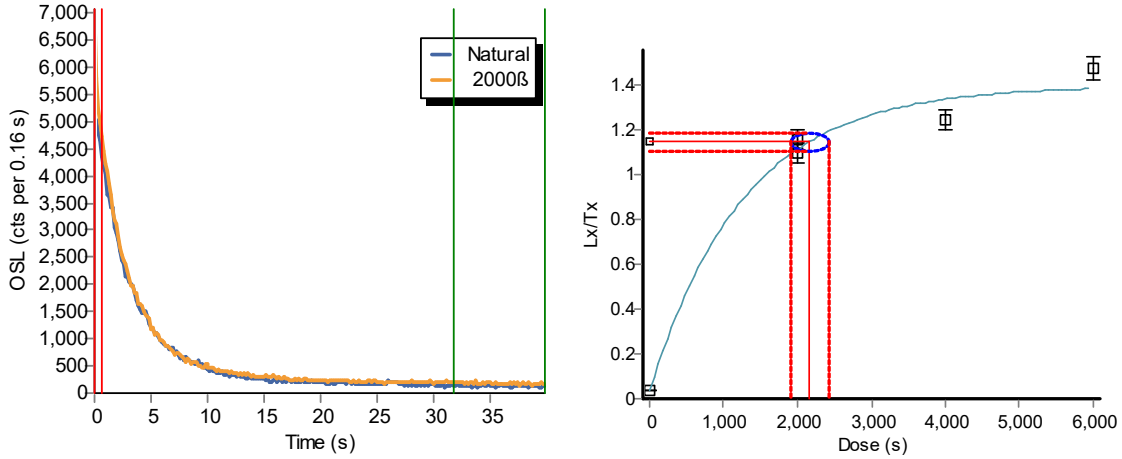
Natural
2000ß
OSL (cts per 0.16 s)
Time (s)
Lx/Tx
Dose (s)

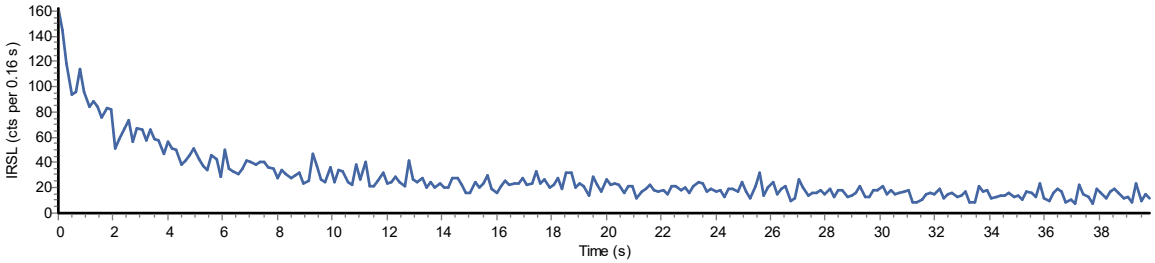
IRSL (cts per 0.16 s)
Time (s)

P4-99m

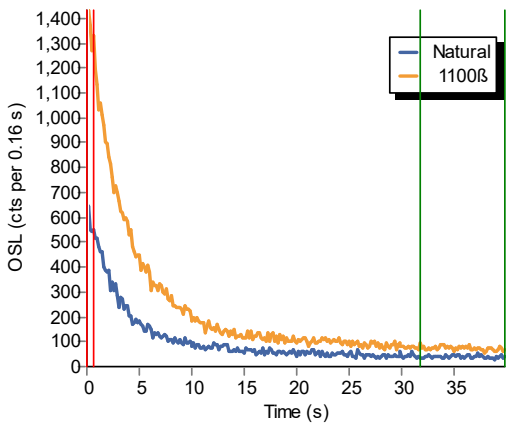
Natural
1100ß
OSL (cts per 0.16 s)
Time (s)

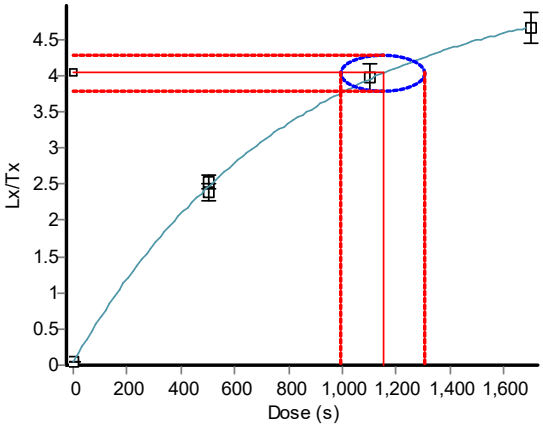
Lx/Tx
Dose (s)

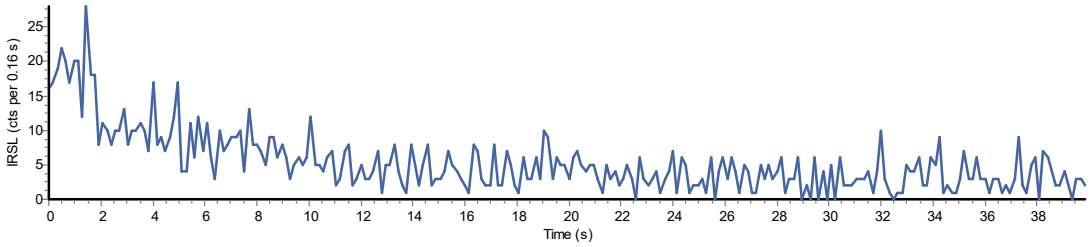
IRSL (cts per 0.16 s)
Time (s)

P6-19m

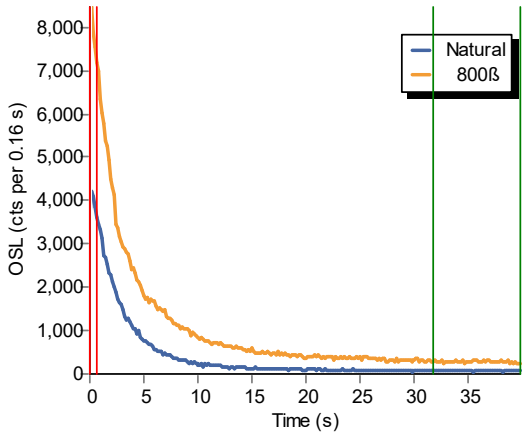
Natural
800ß
OSL (cts per 0.16 s)
Time (s)

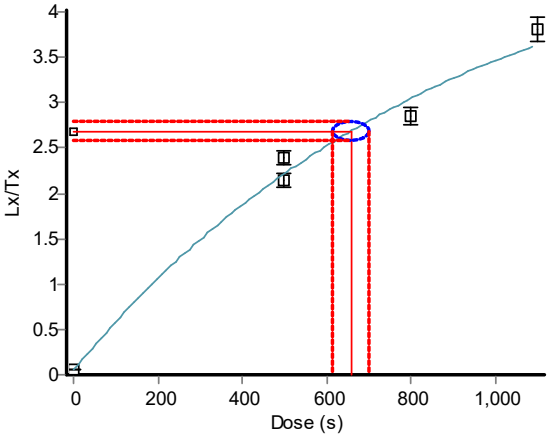
Lx/Tx
Dose (s)

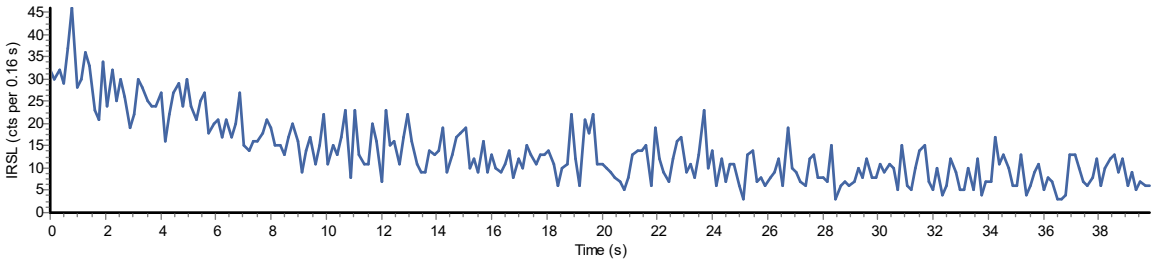
IRSL (cts per 0.16 s)
Time (s)

P6-33m

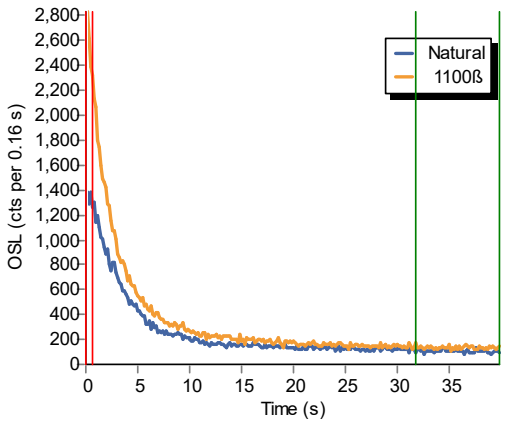
Natural
1100ß
OSL (cts per 0.16 s)
Time (s)

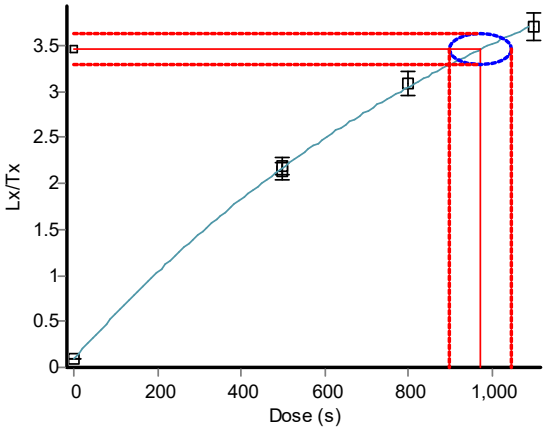
Lx/Tx
Dose (s)

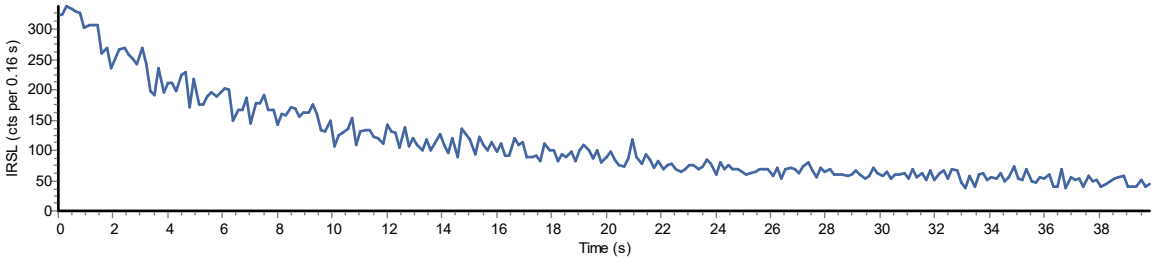
IRSL (cts per 0.16 s)
Time (s)

P6-39m

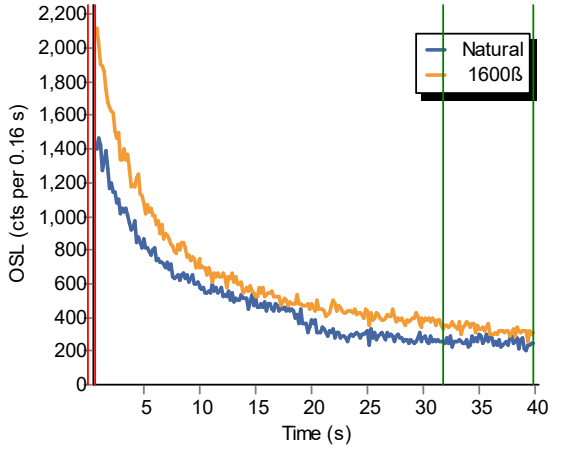
Natural
1600ß
OSL (cts per 0.16 s)
Time (s)

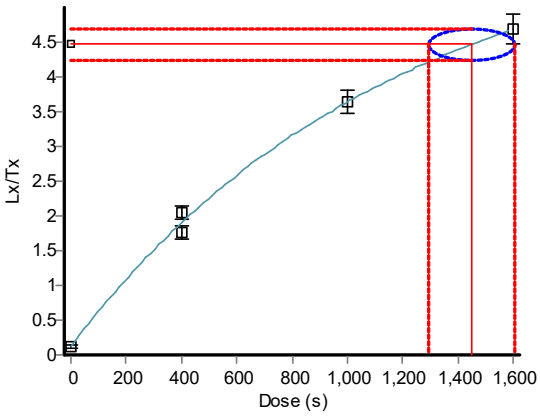
Lx/Tx
Dose (s)

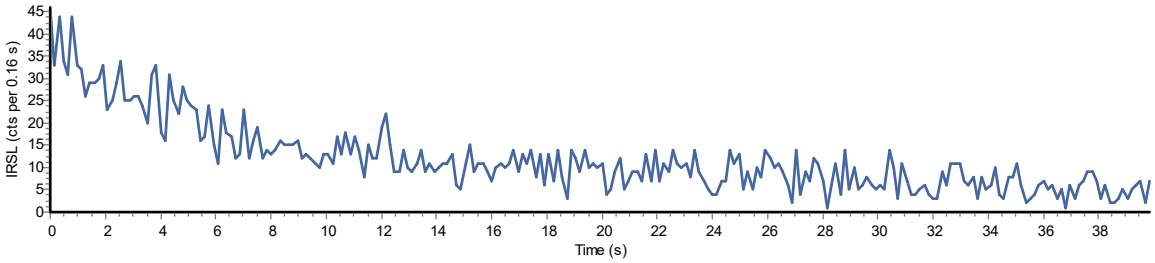
IRSL (cts per 0.16 s)
Time (s)

P6-49m

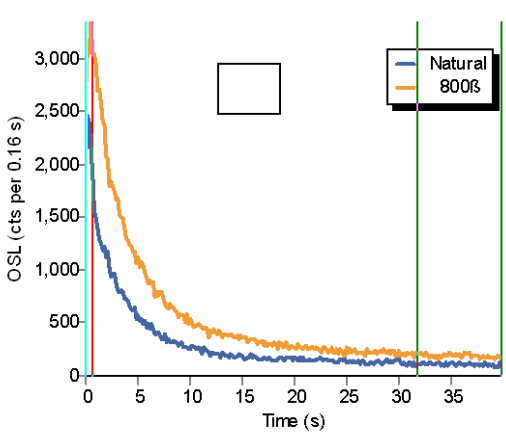
Natural
800ß
OSL (cts per 0.16 s)
Time (s)

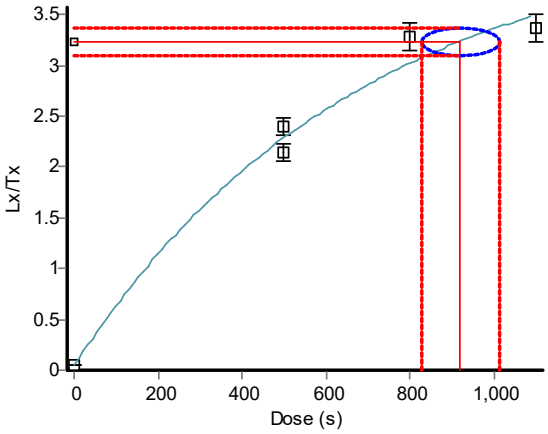
Lx/Tx
Dose (s)

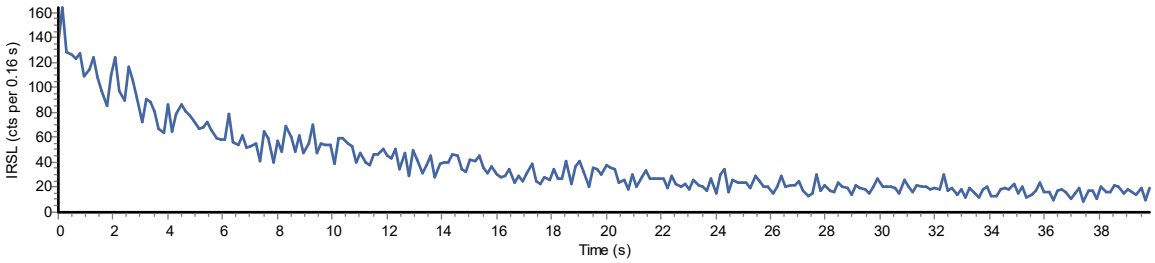
IRSL (cts per 0.16 s)
Time (s)

P7-57m

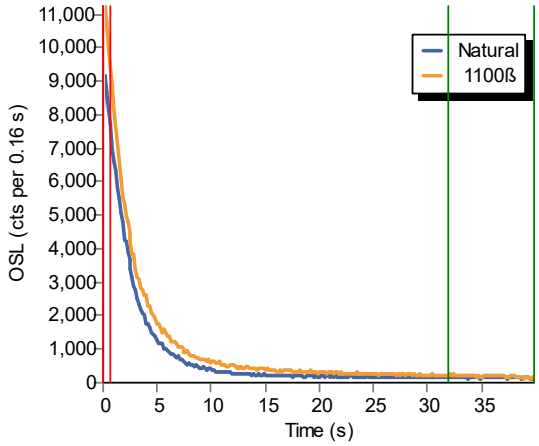
Natural
1100ß
OSL (cts per 0.16 s)
Time (s)

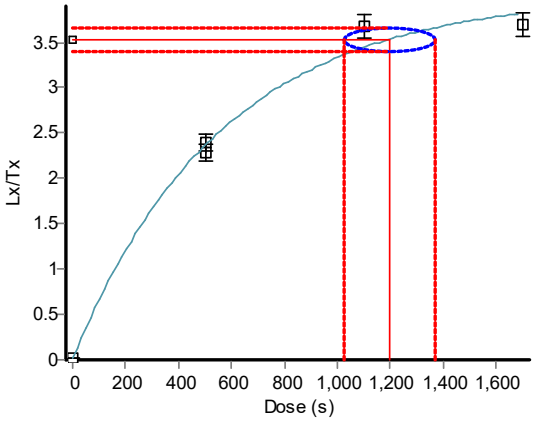
Lx/Tx
Dose (s)

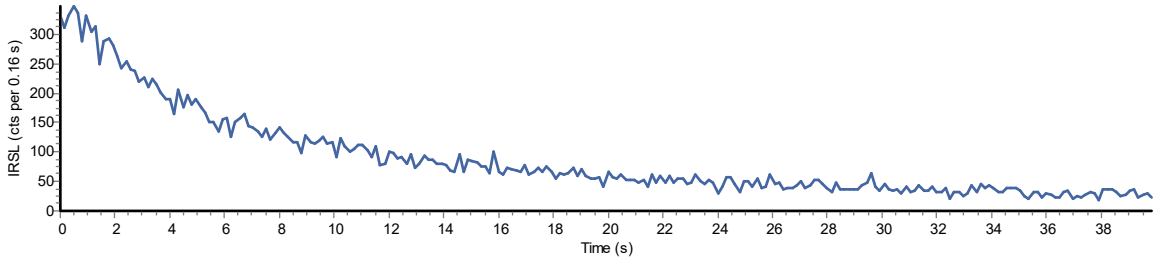
IRSL (cts per 0.16 s)
Time (s)

P7-71m

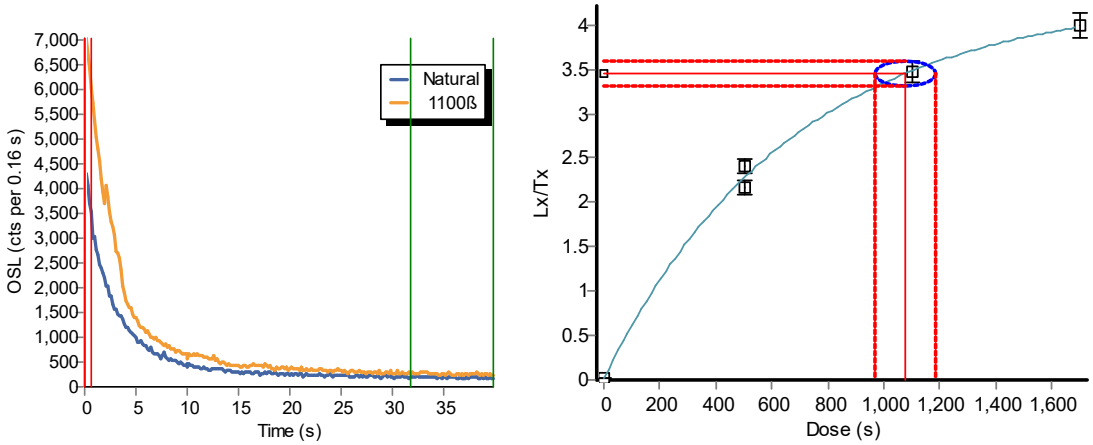
Natural
1100ß
OSL (cts per 0.16 s)
Time (s)
Lx/Tx
Dose (s)

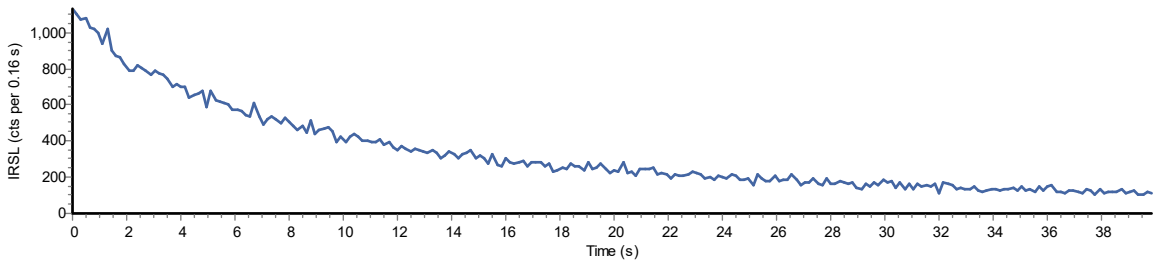
IRSL (cts per 0.16 s)
Time (s)

P9-40m

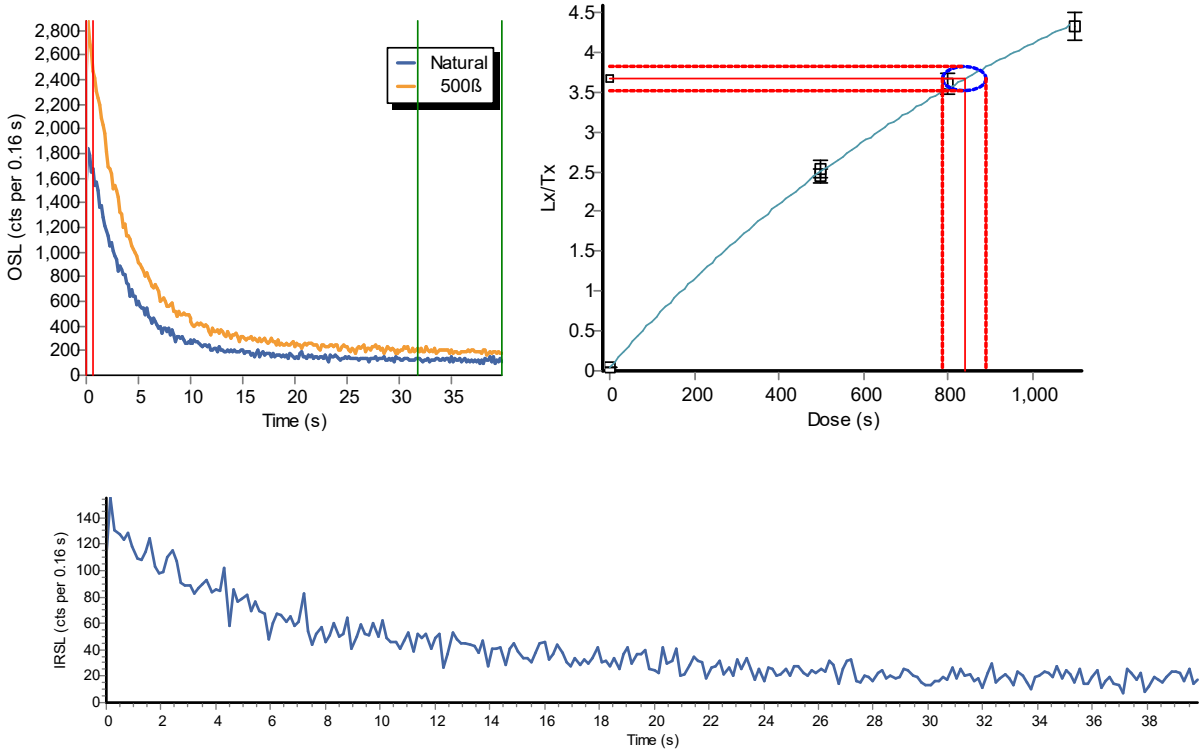

Figure S5. Examples of typical OSL shine down curves (luminescence stimulated in the lab over 40 s of exposure to light) (right panels) and regenerative curves (left panels) for the measured samples. The shine down curves for all aliquots showed fast decay patterns that confirm that the signal is the fast component of luminescence, which is dominant in quartz. Bottom panel shows the decay curve of infrared stimulated luminescence (IRSL).

P3-31M

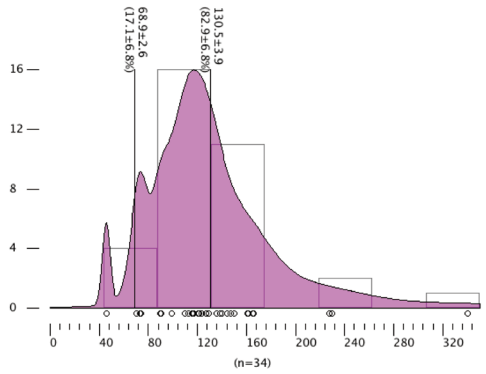

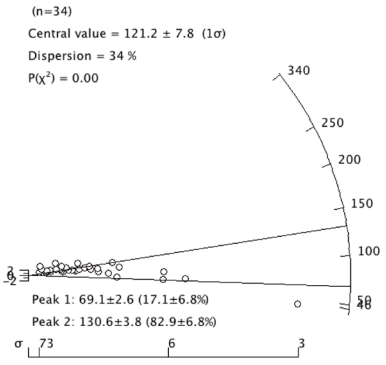

P3-39M

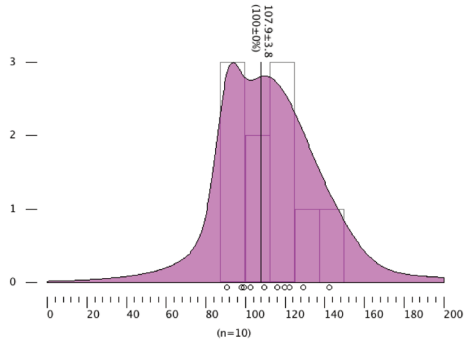

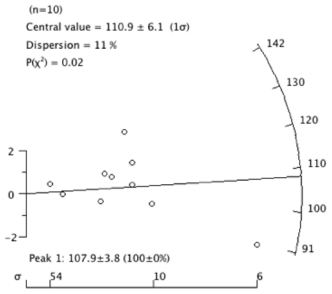

P3-41M

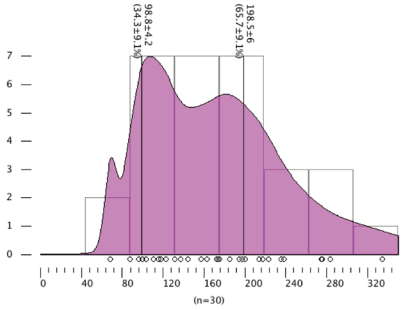

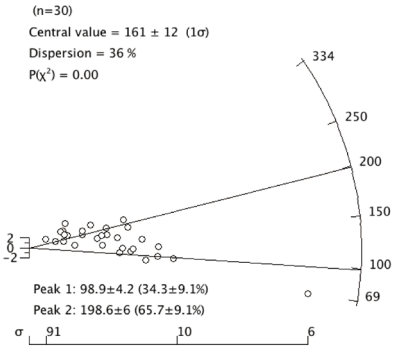

P3-49M

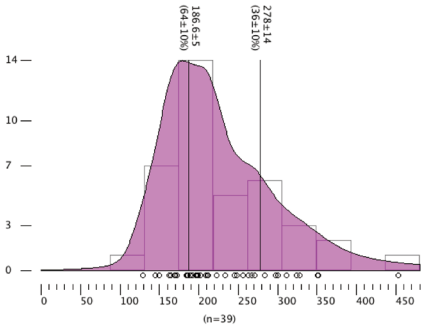

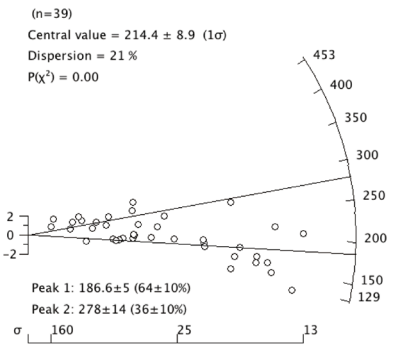

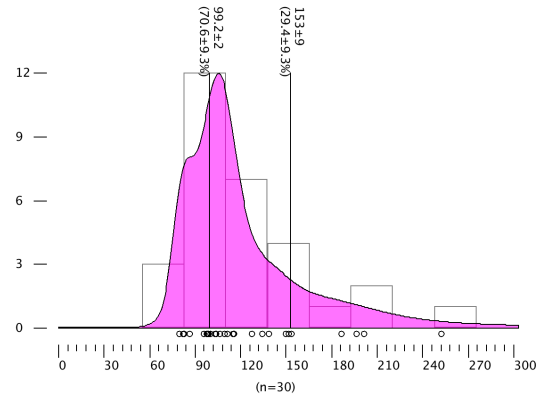
99.2±2
(70.6±9.3%)
153±9
(29.4±9.3%)
12
9
6
3
0
0 30 60 90 120 150 180 210 240 270 300
(n=30)

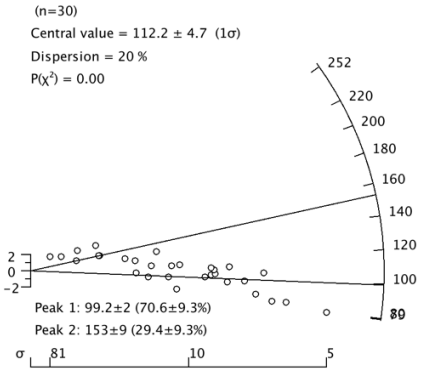
(n=30)
Central value = 112.2 ± 4.7 (1σ)
Dispersion = 20 %
P(χ²) = 0.00
252
220
200
180
160
140
120
100
80
2
0
-2
Peak 1: 99.2±2 (70.6±9.3%)
Peak 2: 153±9 (29.4±9.3%)
σ 81 10 5

P2-23m

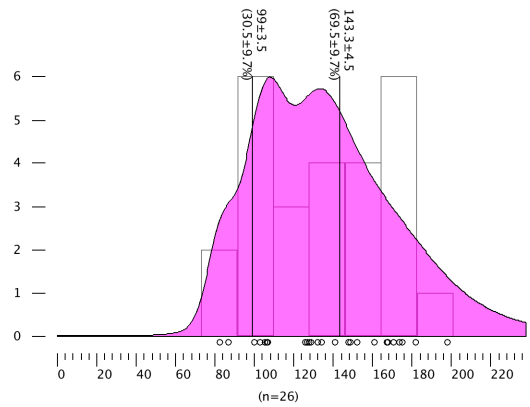
99±3.5
(30.5±9.7%)
143.3±4.5
(69.5±9.7%)
6
5
4
3
2
1
0
0 20 40 60 80 100 120 140 160 180 200 220
(n=26)

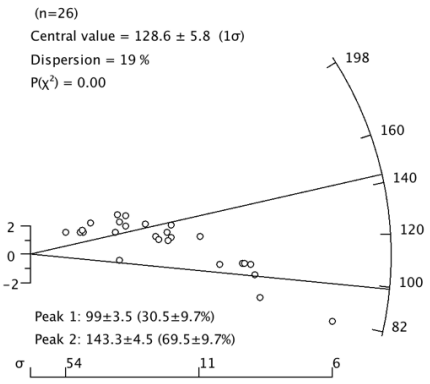
(n=26)
Central value = 128.6 ± 5.8 (1σ)
Dispersion = 19 %
P(χ²) = 0.00
198
160
140
120
100
82
2
0
-2
Peak 1: 99±3.5 (30.5±9.7%)
Peak 2: 143.3±4.5 (69.5±9.7%)
σ 54 11 6

P2-27m

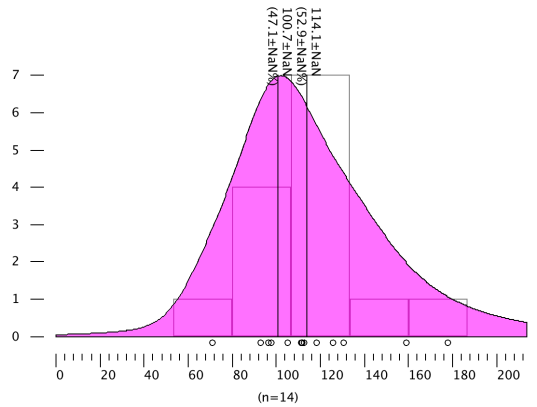
114.1±NaN
(52.9±NaN%)
100.7±NaN
(47.1±NaN%)
0 20 40 60 80 100 120 140 160 180 200
(n=14)

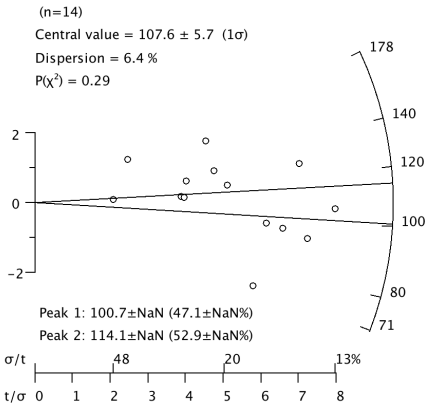
(n=14)
Central value = 107.6 ± 5.7 (1σ)
Dispersion = 6.4 %
P(χ²) = 0.29
178
140
120
100
80
71
Peak 1: 100.7±NaN (47.1±NaN%)
Peak 2: 114.1±NaN (52.9±NaN%)
σ/t 48 20 13%
t/σ 0 1 2 3 4 5 6 7 8

P2-31m

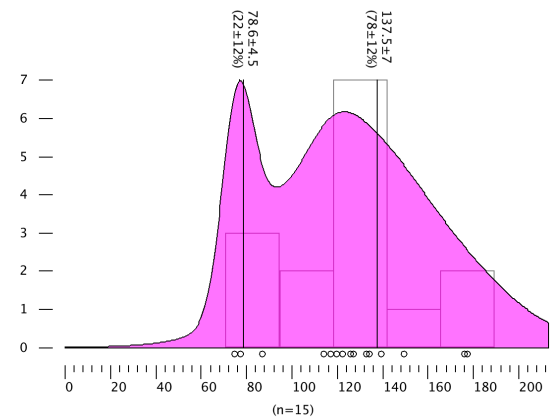
78.6±4.5
(22±12%)
137.5±7
(78±12%)
0 20 40 60 80 100 120 140 160 180 200
(n=15)

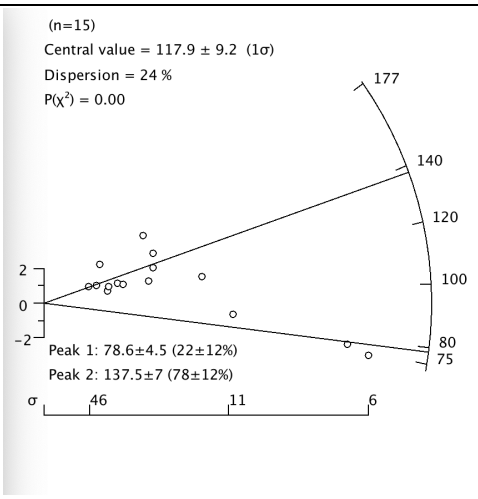
(n=15)
Central value = 117.9 ± 9.2 (1σ)
Dispersion = 24 %
P(χ²) = 0.00
177
140
120
100
80
75
Peak 1: 78.6±4.5 (22±12%)
Peak 2: 137.5±7 (78±12%)
σ 46 11 6

P2-41m

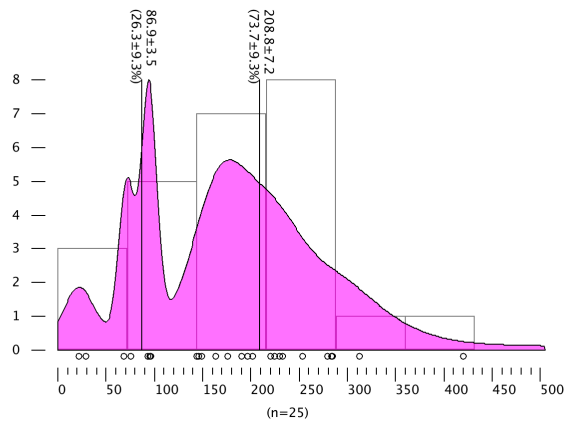
86.9±3.5
(26.3±9.3%)
208.8±7.2
(73.7±9.3%)
0
1
2
3
4
5
6
7
8
0
50
100
150
200
250
300
350
400
450
500
(n=25)

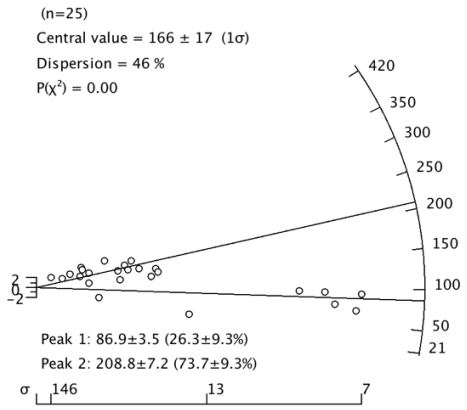
(n=25)
Central value = 166 ± 17 (1σ)
Dispersion = 46 %
P(χ²) = 0.00
420
350
300
250
200
150
100
50
21
2
0
-2
Peak 1: 86.9±3.5 (26.3±9.3%)
Peak 2: 208.8±7.2 (73.7±9.3%)
σ
146
13
7

P3-29m

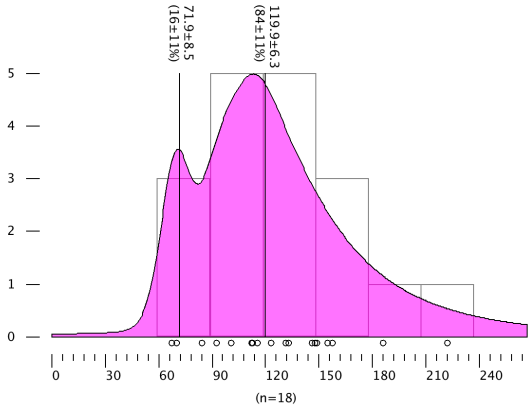
71.9±8.5
(16±11%)
119.9±6.3
(84±11%)
0
1
2
3
4
5
0
30
60
90
120
150
180
210
240
(n=18)

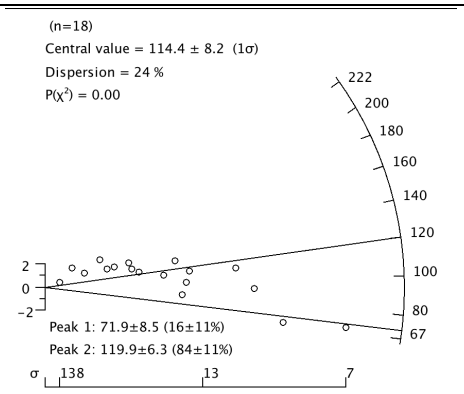
(n=18)
Central value = 114.4 ± 8.2 (1σ)
Dispersion = 24 %
P(χ²) = 0.00
222
200
180
160
140
120
100
80
67
2
0
-2
Peak 1: 71.9±8.5 (16±11%)
Peak 2: 119.9±6.3 (84±11%)
σ
138
13
7

P4-51m

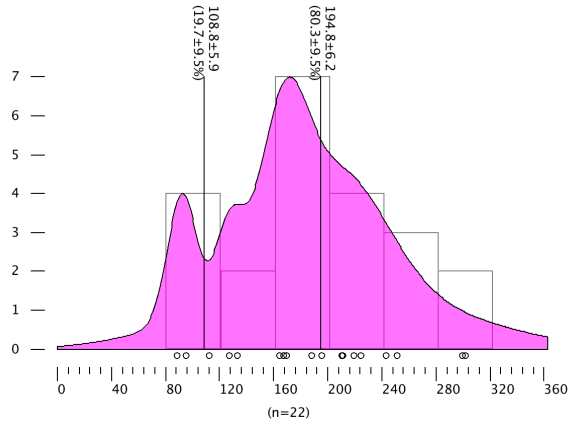
108.8±5.9
(19.7±9.5%)
194.8±6.2
(80.3±9.5%)
(n=22)

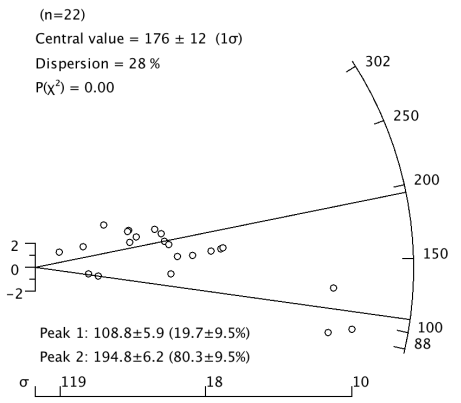
(n=22)
Central value = 176 ± 12 (1σ)
Dispersion = 28 %
P(χ²) = 0.00
Peak 1: 108.8±5.9 (19.7±9.5%)
Peak 2: 194.8±6.2 (80.3±9.5%)
σ 119 18 10

P4-69m

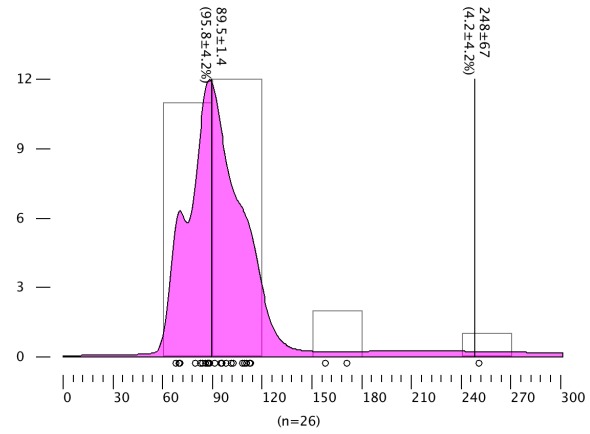
89.5±1.4
(95.8±4.2%)
248±67
(4.2±4.2%)
(n=26)

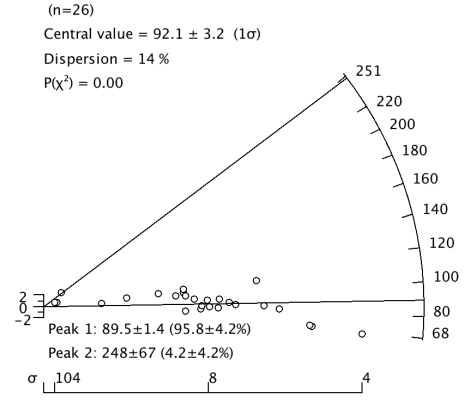
(n=26)
Central value = 92.1 ± 3.2 (1σ)
Dispersion = 14 %
P(χ²) = 0.00
Peak 1: 89.5±1.4 (95.8±4.2%)
Peak 2: 248±67 (4.2±4.2%)
σ 104 8 4

P4-99m

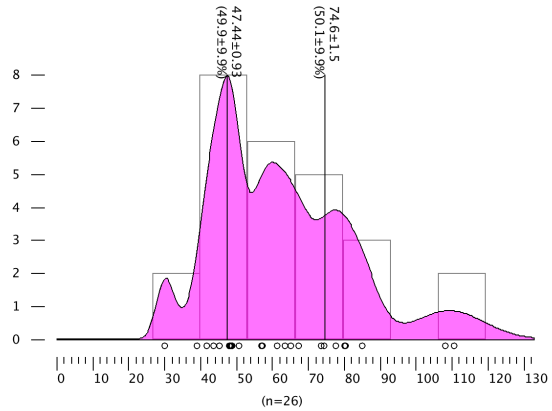
47.44±0.93
(49.9±9.9%)
74.6±1.5
(50.1±9.9%)
0 10 20 30 40 50 60 70 80 90 100 110 120 130
(n=26)

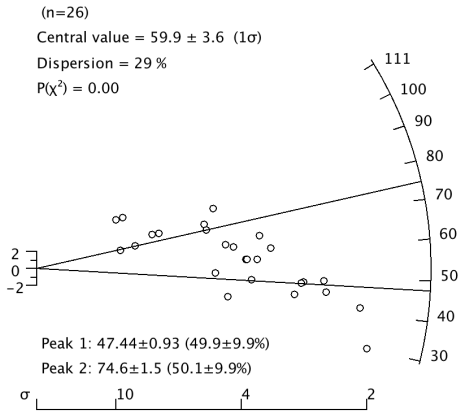
(n=26)
Central value = 59.9 ± 3.6 (1σ)
Dispersion = 29 %
P(χ²) = 0.00
111
100
90
80
70
60
50
40
30
Peak 1: 47.44±0.93 (49.9±9.9%)
Peak 2: 74.6±1.5 (50.1±9.9%)
σ
10
4
2

P6-19m

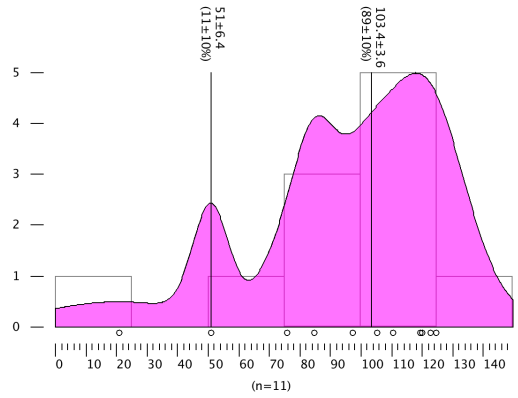
51±6.4
(11±10%)
103.4±3.6
(89±10%)
0 10 20 30 40 50 60 70 80 90 100 110 120 130 140
(n=11)

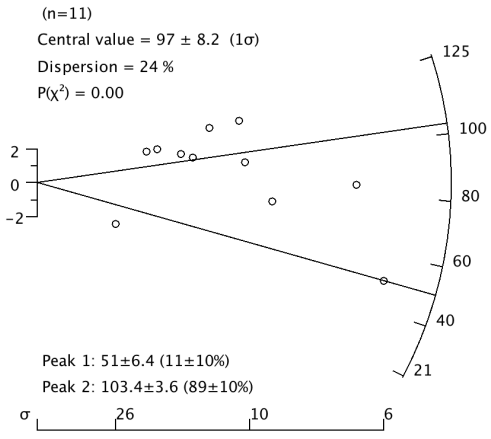
(n=11)
Central value = 97 ± 8.2 (1σ)
Dispersion = 24 %
P(χ²) = 0.00
125
100
80
60
40
21
Peak 1: 51±6.4 (11±10%)
Peak 2: 103.4±3.6 (89±10%)
σ
26
10
6

P6-33m

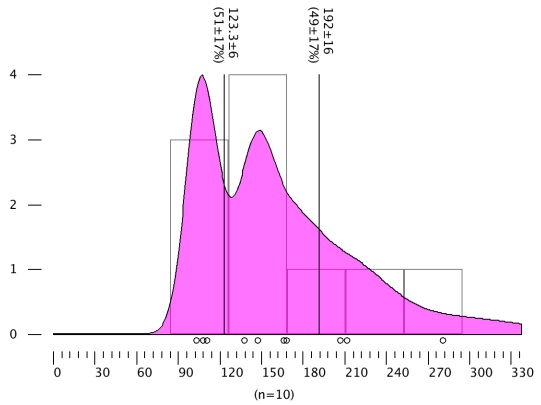
123.3±6
(51±17%)
192±16
(49±17%)
4
3
2
1
0
0 30 60 90 120 150 180 210 240 270 300 330
(n=10)

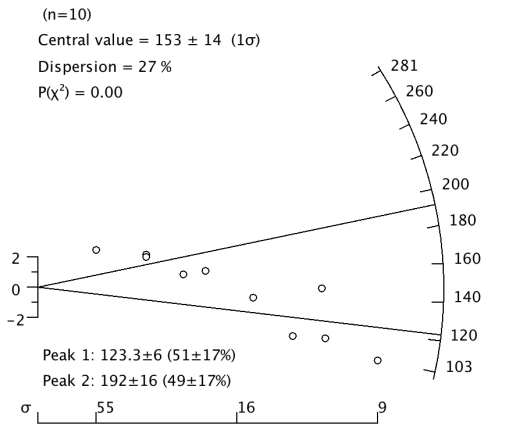
(n=10)
Central value = 153 ± 14 (1σ)
Dispersion = 27 %
P(χ²) = 0.00
281
260
240
220
200
180
160
140
120
103
2
0
-2
Peak 1: 123.3±6 (51±17%)
Peak 2: 192±16 (49±17%)
σ
55
16
9

P6-39m

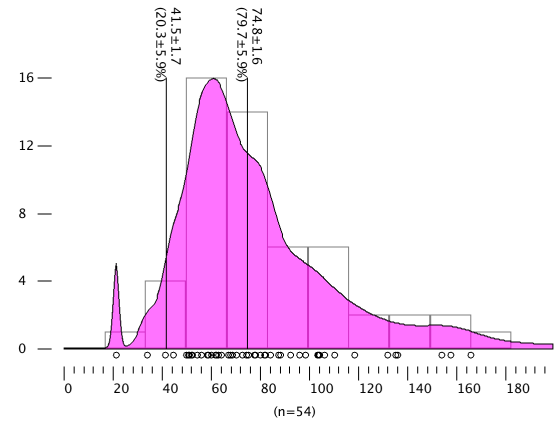
41.5±1.7
(20.3±5.9%)
74.8±1.6
(79.7±5.9%)
16
12
8
4
0
0 20 40 60 80 100 120 140 160 180
(n=54)

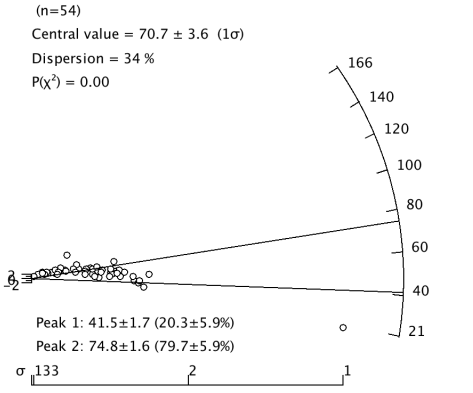
(n=54)
Central value = 70.7 ± 3.6 (1σ)
Dispersion = 34 %
P(χ²) = 0.00
166
140
120
100
80
60
40
21
2
0
-2
Peak 1: 41.5±1.7 (20.3±5.9%)
Peak 2: 74.8±1.6 (79.7±5.9%)
σ
133
2
1

P6-49m

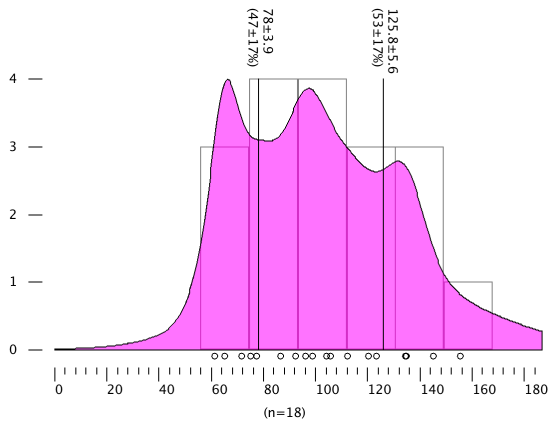
78±3.9
(47±17%)
125.8±5.6
(53±17%)
4
3
2
1
0
0
20
40
60
80
100
120
140
160
180
(n=18)

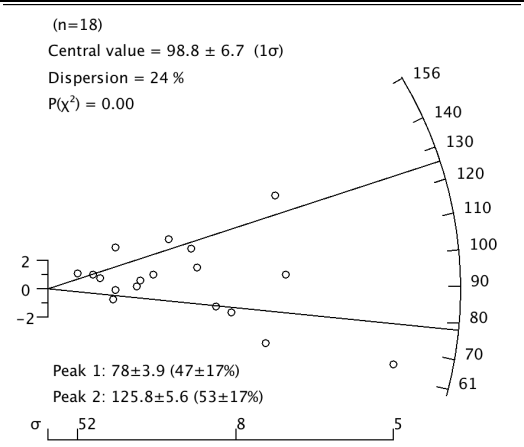
(n=18)
Central value = 98.8 ± 6.7 (1σ)
Dispersion = 24 %
P(χ²) = 0.00
156
140
130
120
110
100
90
80
70
61
2
0
-2
Peak 1: 78±3.9 (47±17%)
Peak 2: 125.8±5.6 (53±17%)
σ
52
8
5

P7-57m

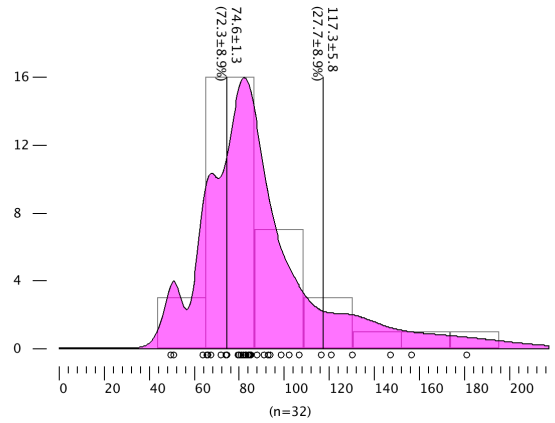
74.6±1.3
(72.3±8.9%)
117.3±5.8
(27.7±8.9%)
16
12
8
4
0
0
20
40
60
80
100
120
140
160
180
200
(n=32)

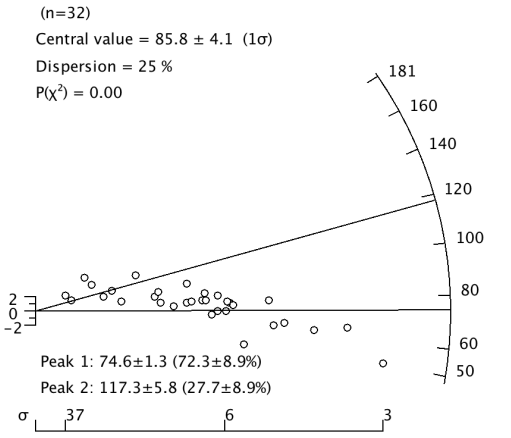
(n=32)
Central value = 85.8 ± 4.1 (1σ)
Dispersion = 25 %
P(χ²) = 0.00
181
160
140
120
100
80
60
50
2
0
-2
Peak 1: 74.6±1.3 (72.3±8.9%)
Peak 2: 117.3±5.8 (27.7±8.9%)
σ
37
6
3

P7-71m

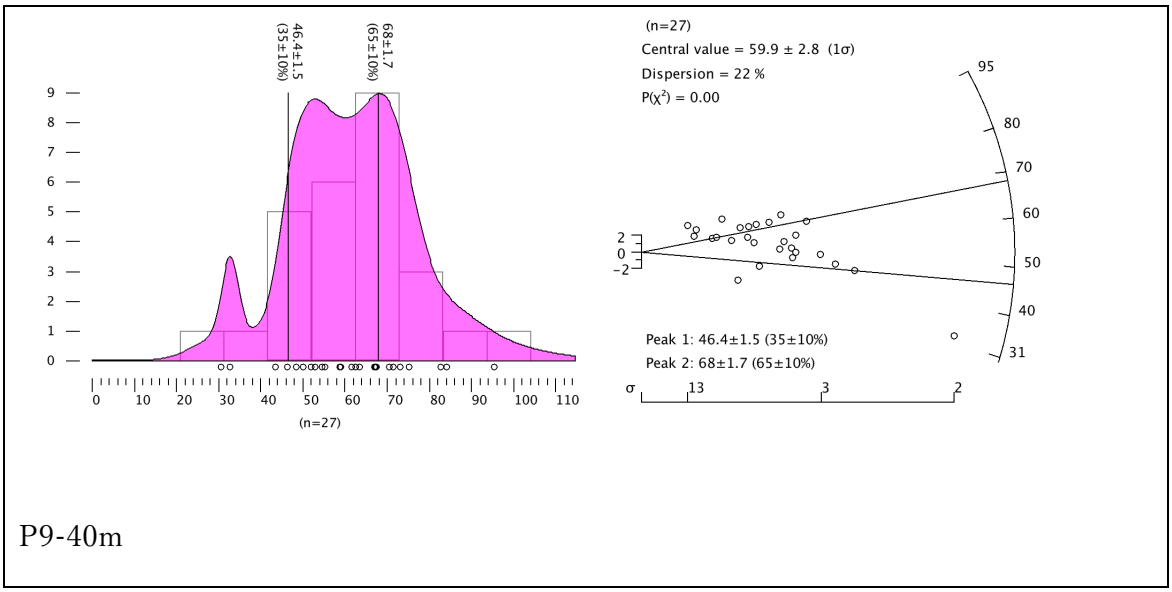

Figure S6. Equivalent doses for measured samples plotted as histograms (number of aliquots) and probability against equivalent dose (Gy) (right panels), and radial plots for each sample using a two-mixing model (left panels). The spread of equivalent dose varies among the samples. A minimum age model separating the population of equivalent dose was employed using a two-mixing model (Vermeesch, 2009). We used the equivalent dose value of the minimum peak from this analysis to calculate the age (Table 2).

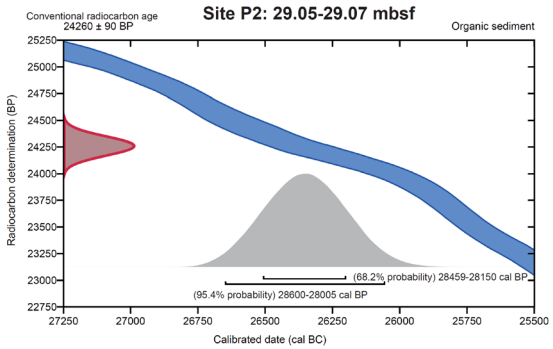
Site P2: 29.05-29.07 mbsf
Conventional radiocarbon age
24260 ± 90 BP
Organic sediment
Radiocarbon determination (BP)
Calibrated date (cal BC)
(68.2% probability) 28459-28150 cal BP
(95.4% probability) 28600-28005 cal BP

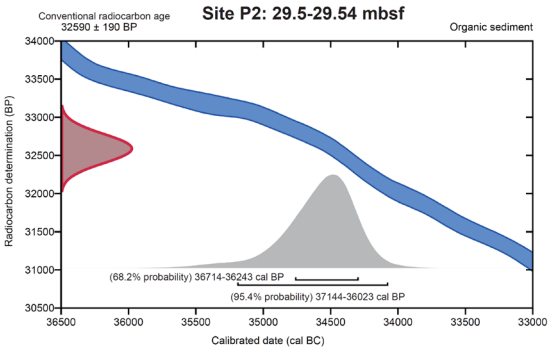
Site P2: 29.5-29.54 mbsf
Conventional radiocarbon age
32590 ± 190 BP
Organic sediment
Radiocarbon determination (BP)
Calibrated date (cal BC)
(68.2% probability) 36714-36243 cal BP
(95.4% probability) 37144-36023 cal BP

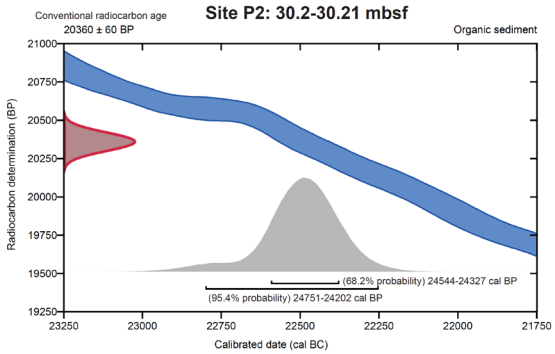
Site P2: 30.2-30.21 mbsf
Conventional radiocarbon age
20360 ± 60 BP
Organic sediment
Radiocarbon determination (BP)
Calibrated date (cal BC)
(68.2% probability) 24544-24327 cal BP
(95.4% probability) 24751-24202 cal BP

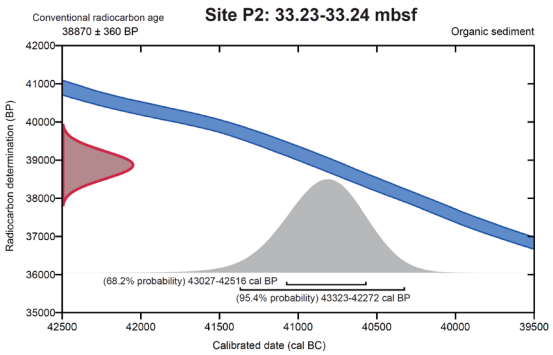
Site P2: 33.23-33.24 mbsf
Conventional radiocarbon age
38870 ± 360 BP
Organic sediment
Radiocarbon determination (BP)
Calibrated date (cal BC)
(68.2% probability) 43027-42516 cal BP
(95.4% probability) 43323-42272 cal BP

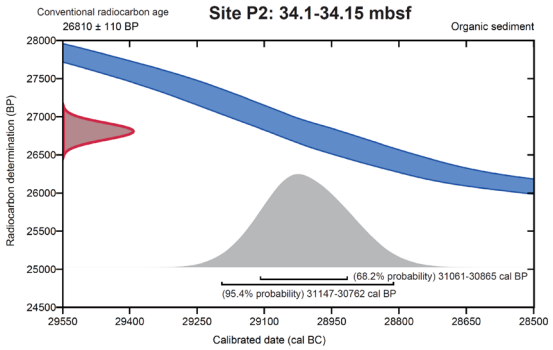
Site P2: 34.1-34.15 mbsf
Conventional radiocarbon age
26810 ± 110 BP
Organic sediment
Radiocarbon determination (BP)
Calibrated date (cal BC)
(68.2% probability) 31061-30865 cal BP
(95.4% probability) 31147-30762 cal BP

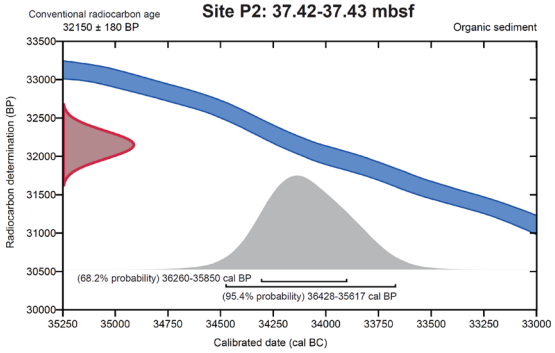
Site P2: 37.42-37.43 mbsf
Conventional radiocarbon age
32150 ± 180 BP
Organic sediment
Radiocarbon determination (BP)
Calibrated date (cal BC)
(68.2% probability) 36260-35850 cal BP
(95.4% probability) 36428-35617 cal BP

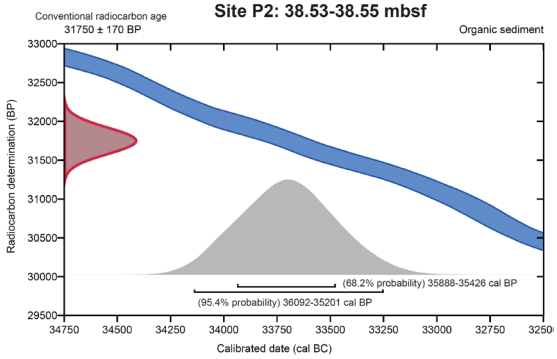
Site P2: 38.53-38.55 mbsf
Conventional radiocarbon age
31750 ± 170 BP
Organic sediment
Radiocarbon determination (BP)
Calibrated date (cal BC)
(68.2% probability) 35888-35426 cal BP
(95.4% probability) 36092-35201 cal BP

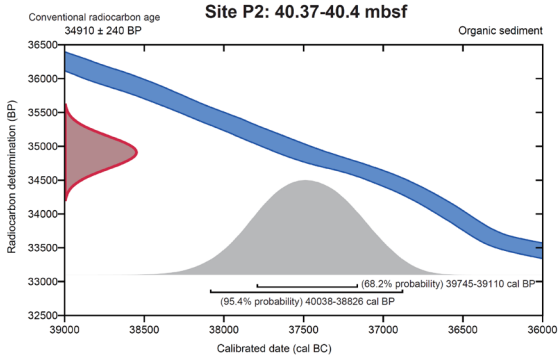
Site P2: 40.37-40.4 mbsf
Conventional radiocarbon age
34910 ± 240 BP
Organic sediment
Radiocarbon determination (BP)
Calibrated date (cal BC)
(68.2% probability) 39745-39110 cal BP
(95.4% probability) 40038-38826 cal BP

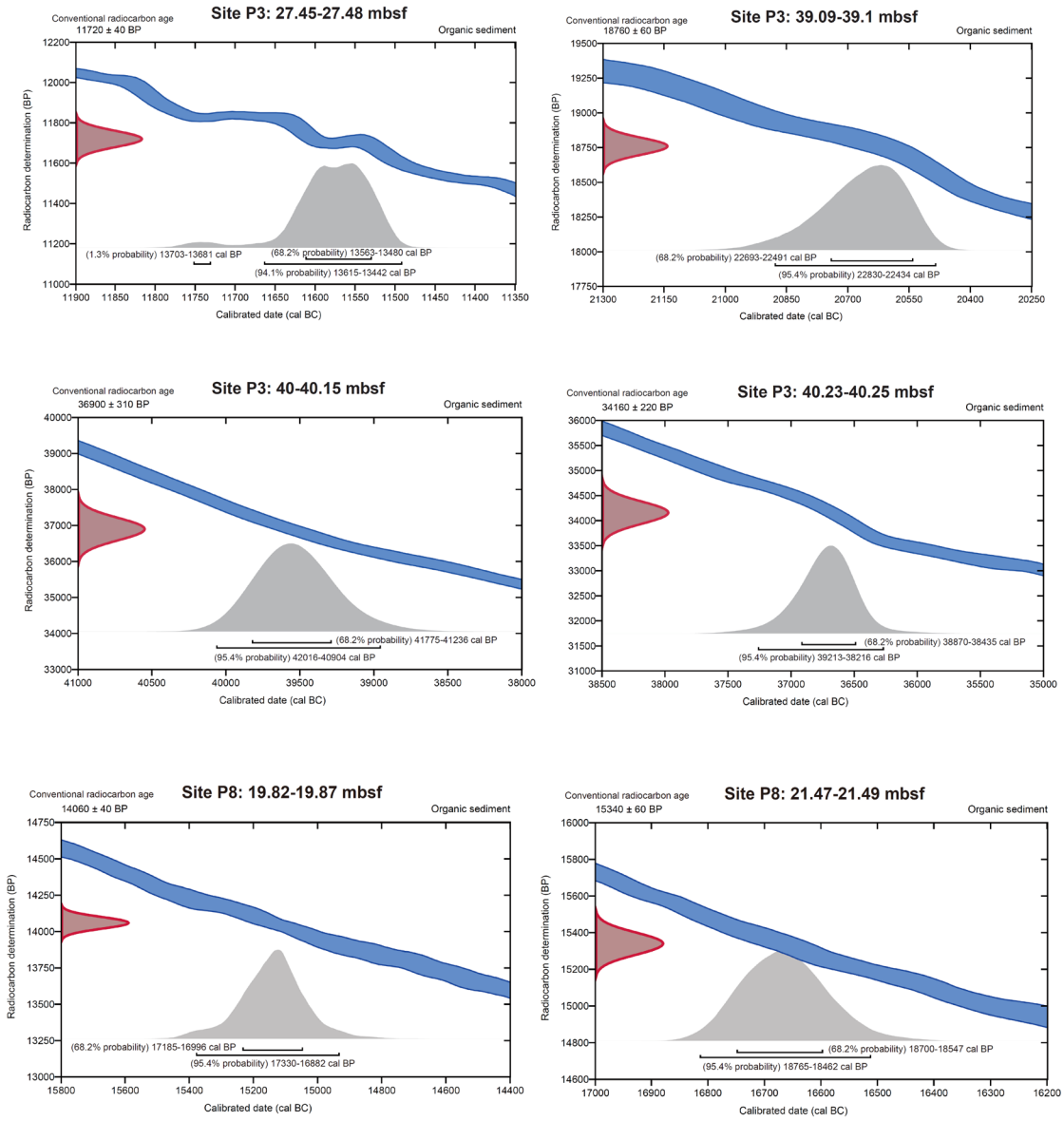

Figure S7. Radiocarbon dating results measured at Beta Analytics Inc., and calibration of radiocarbon age to calendar years for the 18 samples reported in this paper. Sample information is shown above each chart. Calibration of the conventional radiocarbon age

were performed using the 2013 calibration databases (INTCAL13) (Reimer et al., 2013), high probability density range method and Bayesian probability analysis (Ramsey, 2009).

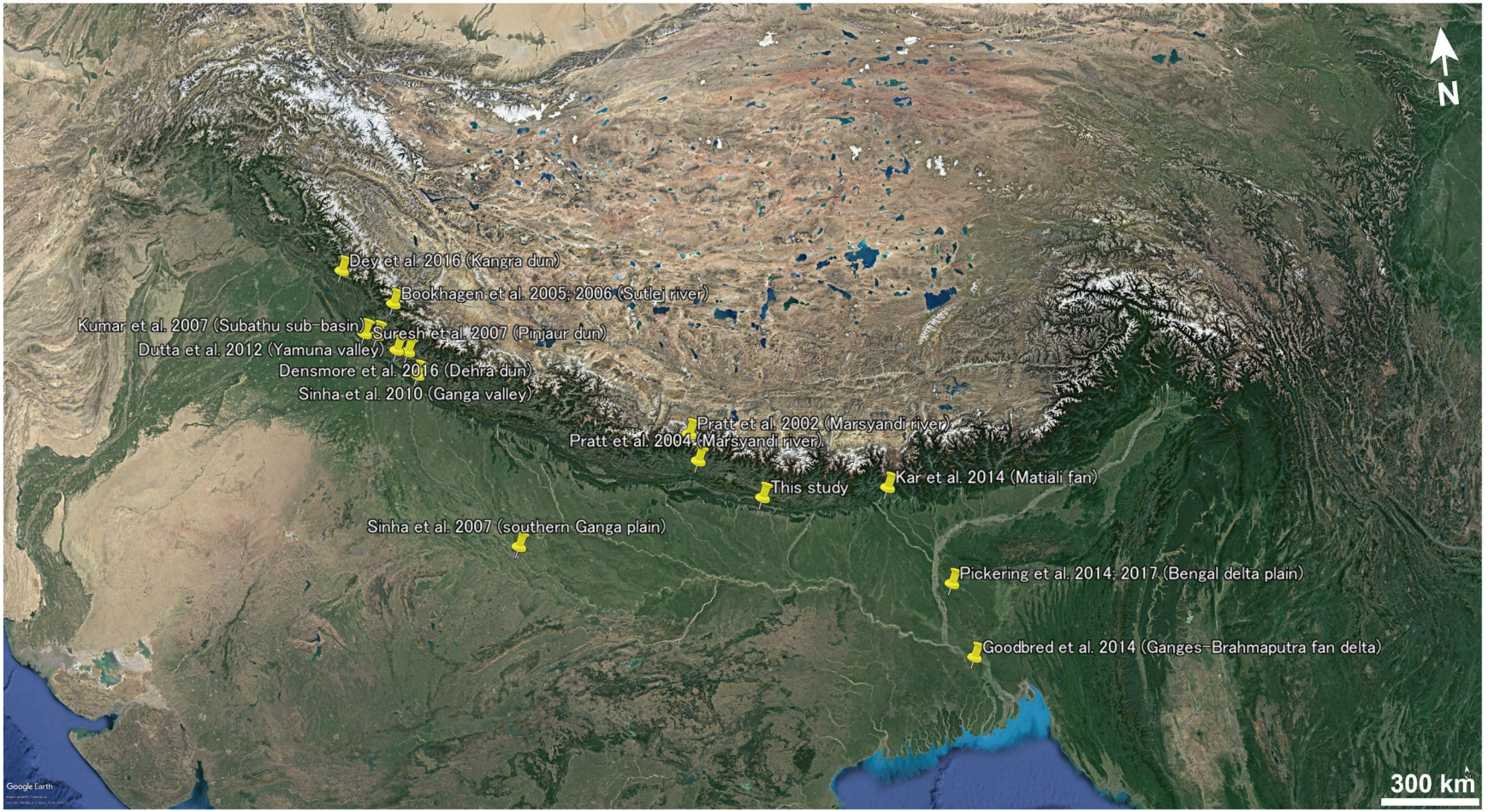
N
Dey et al. 2016 (Kangra dun)
Bookhagen et al. 2005; 2006 (Sutlej river)
Kumar et al. 2007 (Subathu sub-basin)
Suresh et al. 2007 (Pinjaur dun)
Dutta et al. 2012 (Yamuna valley)
Densmore et al. 2016 (Dehra dun)
Sinha et al. 2010 (Ganga valley)
Pratt et al. 2002 (Marsyandi river)
Pratt et al. 2004 (Marsyandi river)
This study
Kar et al. 2014 (Matiali fan)
Sinha et al. 2007 (southern Ganga plain)
Pickering et al. 2014; 2017 (Bengal delta plain)
Goodbred et al. 2014 (Ganges-Brahmaputra fan delta)
Google Earth
300 km

Figure S8. Regional satellite map showing locations of previous studies in other foreland regions (Pratt et al., 2002; 2004; Bookhagen et al., 2005; 2006; Kumar et al., 2007; Sinha et al., 2007; Suresh et al., 2007; Sinha et al., 2010; Dutta et al., 2012; Goodbred et al., 2014; Kar et al., 2014; Pickering et al., 2014; 2017; Densmore et al., 2016; Dey et al., 2016) and this study. Satellite image uses map from Google Earth imagery, Image Landsat/Copernicus.

Dataset S1. Core description sheets for Sites P1-P10, which are the raw data from which we created the core logs in this study. The files contain excel spreadsheets that include our lithological and structural data for each site.

Dataset S2. Geotechnical reports created by the drilling company (Geotech Solutions International Pvt. Ltd.). The files contain drilling procedures, photos, on-site reports, core and sample handling, and on-site logs of the cores.